

Multi-resolution Isogeometric Analysis – Efficient adaptivity utilizing the multi-patch structure

Stefan Takacs*, Stefan Tyoler†

May 2024

Abstract

Isogeometric Analysis (IgA) is a spline based approach to the numerical solution of partial differential equations. There are two major issues that IgA was designed to address. The first issue is the exact representation of domains stemming from Computer Aided Design (CAD) software. In practice, this can be realized only with multi-patch IgA, often in combination with trimming or similar techniques. The second issue is the realization of high-order discretizations (by increasing the spline degree) with numbers of degrees of freedom comparable to low-order methods. High-order methods can deliver their full potential only if the solution to be approximated is sufficiently smooth; otherwise, adaptive methods are required. In the last decades, a zoo of local refinement strategies for splines has been developed. The authors think that many of these approaches are a burden to implement efficiently and impede the utilization of recent advances that rely on tensor-product splines, e.g., concerning matrix assembly and preconditioning. The implementation seems to be particularly cumbersome in the context of multi-patch IgA. Our approach is to moderately increase the number of patches and to utilize different grid sizes on different patches. This allows reusing the existing code bases, recovers the convergence rates of other adaptive approaches and increases the number of degrees of freedom only marginally.

1 Introduction

When Isogeometric Analysis (IgA) was originally proposed almost two decades ago in the seminal paper [10] by Hughes, Cottrell and Bazilevs, it was supposed to solve two major issues. The first issue was that a standard realization of a Finite Element Analysis (FEA) requires the computational domain to be meshed. IgA aims to bridge the gap between Computer Aided Design (CAD) and FEA, allowing to directly use the geometry description from design for analysis. The second goal of IgA was to more easily allow the construction of smooth basis functions. This is of relevance since it reduces the number of degrees of freedom and the number of spurious eigenmodes and it allows the construction of conforming discretizations for fourth and higher order problems. IgA has gained substantial interest since it was first proposed, cf. the book [5] and references therein.

Technically speaking, in IgA one uses B-Splines or Non-Uniform Rational B-Splines (NURBS) as ansatz functions for a Galerkin or collocation discretization of the given boundary value problem.

*stefan.takacs@jku.at, Johannes Kepler University Linz, Austria.

†stefan.tyoler@ricam.oeaw.ac.at, RICAM, Austrian Academy of Sciences, Austria.

This work was supported by the Austrian Science Fund (FWF): P33956

Starting from univariate B-Splines, their extension to two and more dimensions is typically realized by setting up tensor products for the unit square or the unit cube. The basis functions on the computational domain are then defined via the pull-back principle, utilizing a parameterization of the computational domain that may stem from the CAD model. Since the parameterization is required to be continuous, only simply connected domains can be parameterized with a single function. In practice, the overall computational domain is decomposed into subdomains, usually called patches, which are parameterized separately. This approach retains the tensor-product structure and the high smoothness of splines locally. Concerning the global smoothness conditions, one usually only imposes conditions that are necessary in order to obtain a conforming discretization; for second order differential equations, whose conforming discretization is usually posed in the Sobolev space H^1 , only continuity is imposed. Certainly, having only reduced smoothness across the interfaces increases the number of degrees of freedom. However, this is typically negligible; we will elaborate on this in Section 3.

One of the main benefits of a high-order discretization is their superior approximation power, compared to low-order discretizations. For a discretization with polynomial or spline degree p , the approximation error in the standard H^1 Sobolev norm decays like h^p . Certainly, this is only true if the function to be approximated, typically the solution, is smooth enough, specifically it needs to be in the Sobolev space H^{p+1} . So, the higher the chosen degree is, the more smoothness is usually desired for full approximation power.

For many problems, where the desired smoothness is not available globally, it is usually available on large portions of the computational domain. Only close to certain features, like corners or changes in say material parameters, the smoothness of the solution is reduced. This motivates the use of adaptive algorithms that allow for local refinement close to these features. Adaptivity is usually based on the *solve—estimate—mark—refine* loop. After solving the problem on the current discretization, an error estimator is used in order to determine the areas where the mesh is refined. Here, we restrict ourselves to residual based error estimators, cf. [23]. In a next step, certain areas are marked as to be refined, usually with Dörfler marking [6, 16]. Finally, a finer discretization is set up.

In standard finite element contexts, refinement is usually done using simple bisection methods. Since one usually wants to avoid hanging nodes, there are many strategies to avoid them, like red-green based refinement techniques or nearest vertex bisection, cf. [23, 2] to name just a few. Also, in spline contexts, several approaches have been proposed over the last few decades. Among the most prominent examples are hierarchical B-splines (HB) and truncated hierarchical B-splines (THB), see [12, 7, 8] and others, T-splines, see [20], locally refined (LR) splines, see [11] and many others.

There are several targets one wants to achieve with such spline constructions. First of all these splines must offer the desired (local) approximation power, meaning the function space needs to be rich enough. Certainly, this should be possible without introducing too many degrees of freedom. Moreover, the approach needs to be simple enough to be implemented efficiently, including in a multi-patch context.

Most local spline constructions known from literature are formulated for single patch discretizations; often, their generalization to the multi-patch case is a non-trivial task. So, we introduce an approach that is formulated for the multi-patch case straight from the beginning. In order to keep the method simple, we use the multi-patch structure (which we need anyway for the representation of the geometry) also for adaptivity.

In our approach, we keep the local tensor-product structure within each patch. In order to

allow for local refinement, we might decide to refine the B-splines only on a few patches or to split patches into smaller patches, where the grid size could be specified for each of the smaller patches separately. Compared to more standard approaches, this leads to discretizations that are not “fully matching” across the interfaces. One possibility to handle such cases is the use of mortar or discontinuous Galerkin approaches [13, 14]. In our case, the discretizations on the interfaces between any two patches are nested. This allows the use of standard conforming Galerkin discretizations. We show that it is possible to construct bases for the resulting spaces and to provide the desired approximation error estimates.

Besides the fact that our approach is inherently using the multi-patch structure, one of its advantages is that it preserves the local tensor product structure of the problem. So, approaches that rely on this structure, like for matrix assembling, cf. [4, 15] and others, or for preconditioning, cf. [9, 18] and others, can still be used. It is worth stressing again that this approach of splitting patches slightly increases the number of degrees of freedom (since the functions are only C^0 smooth at the interfaces of the patches), however this is not significant and is outweighed by the benefits of our approach.

This paper is organized as follows. In Section 2, we introduce the adaptive refinement strategy that is used throughout this paper. A mathematical specification of the non-conforming multi-patch geometries produced by the adaptive refinement strategy is specified in Section 3. The construction of a basis for the overall function space and its properties are discussed in Section 4. In Section 5, we provide approximation error estimates. Extensive numerical experiments are presented in Section 6. Conclusions are drawn in Section 7.

2 Isogeometric Galerkin method

We are discussing our approach for a simple elliptic model problem with Dirichlet boundary conditions in two dimensions. Aspects of extending the approach to three dimensions are addressed at the end of this paper. We denote the computational domain by $\Omega \subset \mathbb{R}^2$ and assume it to be open, connected and bounded with a Lipschitz continuous boundary $\partial\Omega$. Given a strictly positive diffusion parameter $\nu \in L^\infty(\Omega)$ and a right-hand-side function $f \in L^2(\Omega)$, the problem reads in variational form as follows.

$$\text{Find } u \in H_0^1(\Omega) : \underbrace{\int_{\Omega} \nu \nabla u \cdot \nabla v dx}_{a(u, v) :=} = \underbrace{\int_{\Omega} f v dx}_{\ell(v) :=} \quad \forall v \in H_0^1(\Omega).$$

Here and in what follows, H^k , H_0^k and L^2 are the standard Sobolev and Lebesgue spaces with standard norms $\|\cdot\|_{H^k}$ and $\|\cdot\|_{L^2}$, see [1]. The restriction to the boundary is to be understood in the sense of a trace operator. To discretize this problem, we use multi-patch Isogeometric Analysis.

We assume that the computational domain Ω is composed of K non-overlapping patches Ω_k , i.e.,

$$\overline{\Omega} = \bigcup_{k=1}^K \overline{\Omega_k} \quad \text{with} \quad \Omega_k \cap \Omega_\ell = \emptyset \quad \text{for } k \neq \ell.$$

We assume that the initial configuration is conforming, i.e., the intersection of the closures of any two different patches $\overline{\Omega_k} \cap \overline{\Omega_\ell}$ is either empty, a common corner or a common edge. Here and in what follows, the edge of a patch Ω_k is the image of one of the four sides of the unit square, like

$G_k((0, 1) \times \{0\})$. Alike, the corners of a patch are the images of the four corners of the unit square, like $G_k(0, 0)$. In the adaptive context, this condition is relaxed to Assumption 3.1.

We further assume that each patch Ω_k is parameterized by a bijective geometry mapping $G_k : \widehat{\Omega} \rightarrow \Omega_k$, where $\widehat{\Omega} := (0, 1)^2$ is the *parameter domain*. In standard IgA applications, the mappings G_k are B-splines or NURBS, however, we do not require this for our analysis. The parameterizations have to be sufficiently regular in order to satisfy the following assumption.

Assumption 2.1. We assume that there is a uniform constant $C_G > 0$ and there are characteristic patch sizes $H_k \geq 0$ and smoothness parameters $r_k > 0$ for each of the patches $k = 1, \dots, K$ such that

$$\max_{i \in \{0, \dots, j\}} \|\partial_x^i \partial_y^{j-i} G_k\|_{L^\infty(\widehat{\Omega})} \leq C_G H_k^j \quad \text{for } j = 1, \dots, r_k + 1 \quad \text{and} \quad \|(\nabla G_k)^{-1}\|_{L^\infty(\widehat{\Omega})} \leq C_G H_k^{-1},$$

where ∂_x^i and ∂_y^j denotes the i -th derivative in direction of x or y , respectively. ∇G_k denotes the Jacobian of G_k . Moreover, we assume the same for the restriction of G_k to its parameter lines, i.e.,

$$\|\partial^j g\|_{L^\infty(0,1)} \leq C_G H_k^j \quad \text{for } j = 1, \dots, r_k + 1, \quad \text{and} \quad \|\partial g\|_{L^\infty(0,1)} \leq C_G H_k^{-1}$$

holds for all $g \in \{G_k(x, \cdot) : x \in [0, 1]\} \cup \{G_k(\cdot, y) : y \in [0, 1]\}$, where $|\cdot|$ denotes the Euclidean norm.

For each of the patches, we set up independent function spaces of some spline degree p . For each spatial direction $\delta \in \{1, 2\}$, we assume to have a p -open knot vector, i.e., $\Xi^{(k,\delta)} = (\xi_i^{(k,\delta)})_{i=1}^{n^{(k,\delta)}+p+1}$ with

$$\begin{aligned} \xi_1^{(k,\delta)} &= \xi_2^{(k,\delta)} = \dots = \xi_{p+1}^{(k,\delta)} \leq \xi_{p+2}^{(k,\delta)} \leq \dots \leq \xi_{n^{(k,\delta)}}^{(k,\delta)} \leq \xi_{n^{(k,\delta)}+1}^{(k,\delta)} = \xi_{n^{(k,\delta)}+2}^{(k,\delta)} = \dots = \xi_{n^{(k,\delta)}+p+1}^{(k,\delta)}, \\ \xi_i^{(k,\delta)} &< \xi_{i+p}^{(k,\delta)} \quad \text{for } i = 2, \dots, n^{(k,\delta)}. \end{aligned}$$

For every knot vector, the associated B-spline basis $(B_i^{(k,\delta)})_{i=1}^{n^{(k,\delta)}}$ is given by the Cox-de Boor formula, see [3]. This basis spans the corresponding B-spline function space $\widehat{V}_h^{(k,\delta)} := \text{span}\{B_i^{(k,\delta)} : i = 1, \dots, n^{(k,\delta)}\}$ on the unit interval.

On the parameter domain $\widehat{\Omega} = (0, 1)^2$, we define a corresponding tensor-product basis $\widehat{\Phi}^{(k)} := (\widehat{\phi}_i^{(k)})_{i=1}^{n^{(k)}}$ with $n^{(k)} = n^{(k,1)} n^{(k,2)}$, which is mapped to the physical patch Ω_k via the *pull-back principle* in order to obtain a basis $\Phi^{(k)} := (\phi_i^{(k)})_{i=1}^{n^{(k)}}$:

$$\widehat{\phi}_{i+(j-1)n^{(k,1)}}(x, y) = B_i^{(k,1)}(x) B_j^{(k,2)}(y) \quad \text{and} \quad \phi_j^{(k)}(G_k(\mathbf{x})) = \widehat{\phi}_j^{(k)}(\mathbf{x}).$$

These bases span the spaces $\widehat{V}_h^{(k)} = \text{span}\{\widehat{\phi}_i^{(k)} : i = 1, \dots, n^{(k)}\}$ and $V_h^{(k)} = \text{span}\{\phi_i^{(k)} : i = 1, \dots, n^{(k)}\}$. Based on such a construction, we denote the grid size \widehat{h}_k associated to the parameter domain and the grid size h_k associated to the physical patch via

$$\widehat{h}_k := \max_{\delta \in \{1,2\}} \max_{i \in \{1, \dots, n^{(k,\delta)}\}} \xi_{i+1}^{(k,\delta)} - \xi_i^{(k,\delta)} \quad \text{and} \quad h_k := H_k \widehat{h}_k$$

and analogously the minimum grid size via

$$\widehat{h}_{k,min} := \min_{\delta \in \{1,2\}} \min_{i \in \{1, \dots, n^{(k,\delta)} : \xi_{i+1}^{(k,\delta)} \neq \xi_i^{(k,\delta)}\}} \xi_{i+1}^{(k,\delta)} - \xi_i^{(k,\delta)} \quad \text{and} \quad h_{k,min} := H_k \widehat{h}_{k,min}.$$

The overall function space with grid size $h := \max\{h_1, \dots, h_K\}$ is then

$$V_h := \{v \in H_0^1(\Omega) : v|_{\Omega_k} \in V_h^{(k)}\}. \quad (1)$$

In order for this to be viable, we need that the trace spaces of V_h associated to the edges between any two patches are rich enough. For standard conforming spaces, this is ensured by the concept of *fully matching discretizations*, which guarantees

$$V_h \Big|_{\partial\Omega_k \cap \partial\Omega_\ell} = V_h^{(k)} \Big|_{\partial\Omega_k \cap \partial\Omega_\ell} = V_h^{(\ell)} \Big|_{\partial\Omega_k \cap \partial\Omega_\ell} \quad (2)$$

for any two patches Ω_k and Ω_ℓ sharing an edge.

The problem is then discretized using the Galerkin principle, leading to the following problem:

$$\text{Find } u_h \in V_h : \quad a(u_h, v_h) = \ell(v_h) \quad \forall v_h \in V_h \subset H_0^1(\Omega).$$

An a-priori estimate for the overall discretization error is obtained via Céa's Lemma. If the solution satisfies the regularity assumption $u \in H^{p+1}(\Omega)$, the discretization error $\|u - u_h\|_{H^1(\Omega)}$ decays like h^p . For $p = 1$, H^2 regularity is desired to obtain the full rates that can be expected for uniformly refined B-spline spaces. Regularity theorems guaranteeing H^2 -regularity do not apply at reentrant corners and where the diffusion coefficient ν is discontinuous. For $p \geq 2$, even stronger regularity results are desired, which require even more regularity of the data. In order to recover the optimal rates (with respect to the number of degrees of freedom), adaptive meshing in terms of the grid size is the method of choice.

3 Adaptivity and non-conforming multi patch discretization

In order to steer adaptive refinement, we use local error estimators to assess the energy error on each of the patches. So, we compute for each patch the value

$$\eta_k^2 := h_k^2 \|f + \operatorname{div}(\nu \nabla u)\|_{L^2(\Omega_k)}^2 + \sum_{\ell} \frac{h_k}{2} \|\mathbf{n} \cdot ((\nu \nabla u_h)|_{\Omega_k} - (\nu \nabla u_h)|_{\Omega_\ell})\|_{L^2(\partial\Omega_k \cap \partial\Omega_\ell)}^2, \quad (3)$$

where the sum is taken for all indices ℓ referring to a patch Ω_ℓ that shares an edge with Ω_k and \mathbf{n} is the unit normal vector. As a next step, we use Dörfler marking to mark the patches to be refined. As already mentioned, we are interested in methods that preserve the local tensor-product structure on each of the patches. There are several ways this can be achieved. The simplest option would be to refine the grids on all of the marked patches. While this is possible, it does not give the possibility to obtain a sufficiently fine-grained refinement towards singularities.

So, we apply the following strategy; However, many alternatives are possible that fit in the theoretical framework presented in this paper. For each marked patch, say Ω_k , we first apply dyadic refinement, i.e., we construct a finer space $V_{h/2}^{(k)}$ by introducing new knots in the middle between any two non-equal knots in the knot vectors $\Xi^{(k,1)}$ and $\Xi^{(k,2)}$. Secondly, we subdivide (split) the marked patch into four sub-patches $\Omega_{k,i} := G_{k,i}(\hat{\Omega})$ with

$$\begin{aligned} G_{k,1}(x, y) &= G_k(\tfrac{1}{2}x, \tfrac{1}{2}y), & G_{k,2}(x, y) &= G_k(\tfrac{1}{2}(x+1), \tfrac{1}{2}y), \\ G_{k,3}(x, y) &= G_k(\tfrac{1}{2}x, \tfrac{1}{2}(y+1)), & G_{k,4}(x, y) &= G_k(\tfrac{1}{2}(x+1), \tfrac{1}{2}(y+1)). \end{aligned} \quad (4)$$

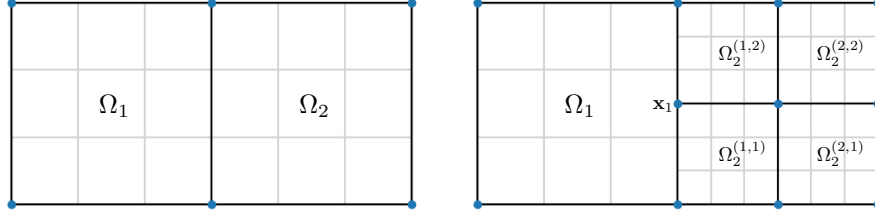


Figure 1: Local refinement of patch Ω_2 .

The associated function spaces are then $V_{h/2}^{(k,i)} := \{v|_{\tilde{\Omega}_{k,i}} : v \in V_h^{(k)}\}$, see Figure 1 for an example, where Ω_2 is subdivided. After refinement, all resulting patches are again enumerated, like $\tilde{\Omega}_1, \dots, \tilde{\Omega}_5$ in the figure. By using this refinement strategy, the number of degrees of freedom (per patch) is kept almost unchanged; we have $\hat{h}_{k,i} \approx \hat{h}_k$ for $i \in \{1, 2, 3, 4\}$.

The diameters of the patches $\tilde{\Omega}_{k,i}$ are (up to multiplicative constants depending on C_S from Assumption 2.1) half the diameter of the patch Ω_k . Indeed, we have

Lemma 3.1. *Provided that the geometry representation satisfies Assumption 2.1 and the patch Ω_k is replaced by the patches $\tilde{\Omega}_{k,i} := \tilde{G}_{k,i}(\tilde{\Omega})$ with $\tilde{G}_{k,i}$ as in (4) for $i \in \{1, 2, 3, 4\}$, then the new geometry representation satisfies Assumption 2.1 with the same constant C_G and $\tilde{H}_{k,i} = \frac{1}{2}H_k$.*

Proof. Follows from simple scaling arguments and $\|\cdot\|_{L^\infty(\tilde{\Omega})} \leq \|\cdot\|_{L^\infty(\tilde{\Omega})}$ for $\tilde{\Omega} \subseteq \tilde{\Omega}$. \square

As already mentioned, we assume that the initial configuration is matching, i.e., that for any two different patches, $\Omega_k \cap \Omega_\ell$ is either empty, a common corner or a common edge. By applying a splitting approach as introduced in (4), this condition is not retained, since corners of one patch can be located on the edge of a neighboring patch; we call such corners *T-junctions*. In the example depicted in Figure 1, the vertex \mathbf{x}_1 would be an example for a T-junction. Our refinement strategy guarantees that the following assumptions are satisfied.

Assumption 3.1. The intersection of the closures of any two different patches, i.e., $\overline{\Omega_k} \cap \overline{\Omega_\ell}$, is either (a) empty, (b) a vertex of (at least) one of the two patches, or (c) an edge of (at least) one of the two patches.

Assumption 3.2. No T-junction is located on $\partial\Omega$ and any two patches meeting in a T-junction share an edge.

As mentioned in the last section, we assume (2) for the initial configuration. If only one of the patches adjacent to an edge is refined, the condition (2) is not satisfied anymore. However, the trace spaces of the neighboring patches are nested, cf. Figure 1. So, the following assumption holds.

Assumption 3.3. For any two patches Ω_k and Ω_ℓ sharing an edge, we have

$$V_h^{(k)}|_{\partial\Omega_k \cap \partial\Omega_\ell} \subseteq V_h^{(\ell)}|_{\partial\Omega_k \cap \partial\Omega_\ell} \quad \text{or} \quad V_h^{(\ell)}|_{\partial\Omega_k \cap \partial\Omega_\ell} \subseteq V_h^{(k)}|_{\partial\Omega_k \cap \partial\Omega_\ell}.$$

This configuration guarantees that the trace space is rich enough and does not degenerate the approximation quality of the discrete space. This assumption is also valid after any further refinement

step. This is obvious if both patches adjacent to an edge are refined or if the patch is refined which already has a finer grid. Assumption 3.3 is also true if the patch with the coarser grid is refined (like if one would refine Ω_1 in the example depicted in Figure 1) since the finer grid is the result of the application of the refinement procedure and the application of the same procedure to the coarser grid yields the same result.

For the approximation error estimates, we need the following assumption that guarantees that the edges are not too small, compared to the grid sizes of the adjacent patches.

Assumption 3.4. For any two patches Ω_k and Ω_ℓ , sharing an edge, the length of its pre-image is at least as large as p times the local grid size, i.e., $|G_k^{-1}(\partial\Omega_k \cap \partial\Omega_\ell)| \geq p \hat{h}_k$.

This condition can be ensured by guaranteeing that the local grid size disparity is not too large.

A minor drawback of this patch-wise splitting approach in comparison to alternative spline based local refinement methods is the increase of degrees of freedom, emerging from the introduction of additional (only continuous) interfaces. Since we assume to have at least p^d knots per patch, where d is the spatial dimension, this only moderately increases the number of degrees of freedom. If the number of knots were significantly larger this increase would even be negligible.

4 Construction of a basis

Although the definition (1) of the global function space V_h is simple, its representation in form of a basis is not straightforward, especially for the not fully matching case. We construct a basis Φ for the global space by building linear combinations of the basis functions in the bases $\Phi^{(k)}$ of the local spaces $V_h^{(k)}$. For this purpose we represent the continuity of functions in V_h in terms of constraints.

A function u_h that is patch-wise defined by $u_h|_{\Omega_k} = \sum_{i=1}^{n^{(k)}} u_i^{(k)} \phi_i^{(k)} \in V_h^{(k)}$ is in the global space V_h if and only if it is continuous. The continuity can be expressed as constraints on the coefficient vectors $\underline{u}_h^{(k)} = (u_1^{(k)}, \dots, u_{n^{(k)}}^{(k)})^\top$. We construct such constraints on an edge-to-edge basis, allowing also redundant constraints. Consider an edge $\Gamma_{k,\ell} := \partial\Omega_k \cap \partial\Omega_\ell$. Both, the bases $\Phi^{(k)}$ and $\Phi^{(\ell)}$, can be restricted to that edge yielding trace bases $\Phi^{(k)}|_{\Gamma_{k,\ell}} := \{\phi_i^{(k)} : \phi_i^{(k)}|_{\Gamma_{k,\ell}} \neq 0\}$ and $\Phi^{(\ell)}|_{\Gamma_{k,\ell}}$, defined analogously. Using Assumption 3.3, we know that – if the two trace bases do not agree anyway – the basis functions in one of them, say $\Phi^{(k)}|_{\Gamma_{k,\ell}}$, can be represented as a linear combination of the basis functions in $\Phi^{(\ell)}|_{\Gamma_{k,\ell}}$:

$$\phi_i^{(k)} = \sum_{j=1}^{n^{(\ell)}} E_{i,j}^{(k,\ell)} \phi_j^{(\ell)} \quad \text{holds on } \Gamma_{k,\ell} \text{ for all } \phi_i^{(k)} \in \Phi^{(k)}|_{\Gamma_{k,\ell}}. \quad (5)$$

The coefficients $E_{i,j}^{(k,\ell)}$ are non-negative and can be constructed by knot insertion algorithms, [3]. Since B-splines interpolate on the boundary, the continuity of the mentioned function u_h can be expressed by

$$u_i^{(k)} - \sum_{j=1}^{n^{(\ell)}} E_{i,j}^{(k,\ell)} u_j^{(\ell)} = 0 \quad \text{for all } \Omega_k \text{ and } \Omega_\ell \text{ sharing an edge and all } i \text{ with } \phi_i^{(k)} \in \Phi^{(k)}|_{\Gamma_{k,\ell}}. \quad (6)$$

All of these constraints can be collected in matrices C_k such that (6) is equivalent to

$$\sum_{k=1}^K C_k \underline{u}_h^{(k)} = 0.$$

By collecting $C := (C_1, \dots, C_K)$ and $\underline{u}_h^\top = (\underline{u}_h^{(1)\top}, \dots, \underline{u}_h^{(K)\top})^\top \in \mathbb{R}^{n^{(pw)}}$, the condition reduces to

$$C \underline{u}_h = 0.$$

By construction, we know that each row of C has exactly one positive coefficient, which is always 1. Since the constraints might be redundant, the matrix might not have full rank.

As mentioned, the basis functions ϕ_i in the global basis Φ are linear combinations of the local basis functions:

$$\phi_i|_{\Omega^{(k)}} = \sum_{j=1}^{n^{(k)}} B_{i,j}^{(k)} \phi_j^{(k)}$$

with coefficients $B_{i,j}^{(k)}$ to be determined. Using

$$B_k := [B_{i,j}^{(k)}]_{i=1, \dots, n^{(k)}} \in \mathbb{R}^{n^{(k)} \times n^{(k)}} \quad \text{and} \quad B = (B_1^\top, \dots, B_K^\top)^\top \in \mathbb{R}^{n \times n^{(pw)}},$$

the problem of finding a basis can be rewritten as a problem on matrices. We are interested in a (full-rank) matrix B whose image is the nullspace of the matrix C , namely

$$\text{nullspace } C = \text{image } B. \tag{7}$$

Moreover, it should satisfy the desirable properties of the B-spline bases, namely the partition of unity, the non-negativity and the local support. These conditions translate to conditions on the matrix B :

$$\sum_{j=1}^n B_{i,j} = 1 \quad \text{for all } i = 1, \dots, n^{(pw)} \text{ (partition of unity),} \tag{8}$$

$$B_{i,j} \geq 0 \quad \text{for all } i = 1, \dots, n^{(pw)} \text{ and } j = 1, \dots, n \text{ (non-negativity).} \tag{9}$$

Moreover, the basis function should have a uniformly bounded support, i.e., each row of B should only have a limited number of non-zero coefficients.

For simple setups, it is possible to derive a matrix B satisfying these properties directly, i.e., it is possible to specify the resulting basis explicitly, this approach is hard to generalize to more involved situations, like three dimensional problems. Moreover, such direct approaches tend to be hard to implement. The following algorithm allows to construction of the matrix B from the constraint matrix C . The matrix is a variant of Gaussian elimination, where the row is chosen in a way such that a rather small fill-in is expected.

Algorithm 4.1.

- Let $B^{(0)} \in \mathbb{R}^{n^{(pw)} \times n^{(pw)}}$ be an identity matrix.
- For $\nu = 1, 2, \dots$ loop until $CB^{(\nu)} = 0$:

- Let $\mathcal{F}_m(C) := \{n : |C_{m,n}| \neq 0, C_{m,n}C_{m,j} \leq 0 \text{ for all } j \neq n\}$. Choose m_ν and n_ν such that

$$n_\nu \in \mathcal{F}_{m_\nu}(CB^{(\nu-1)}) \quad (10)$$

and set

$$R^{(\nu)} := I - \frac{1}{\underline{e}_{m_\nu}^\top CB^{(\nu-1)} \underline{e}_{n_\nu}} \underline{e}_{n_\nu} \underline{e}_{m_\nu}^\top CB^{(\nu-1)}. \quad (11)$$

- Set $B^{(\nu)} := B^{(\nu-1)}R^{(\nu)}$.

- Return the matrix B composed of the non-zero columns of $B^{(N)}$, where N is the last index ν of the loop (i.e., such that $CB^{(N)} = 0$).

The set $\mathcal{F}_m(C)$ contains the index of the sole positive coefficient of the i -th row (if existing) and the index of the sole negative coefficient of the i -th row (if existing). The set might be empty, if the i -th row vanishes or if there are several positive and several negative coefficients in that row. We will show later that there is at least one row m_ν such that $\mathcal{F}_{m_\nu}(CB^{(\nu-1)})$ is not empty (Lemma 4.5). First, we show that the derived representation of the global basis has the desired properties.

Lemma 4.1. *The returned matrix B has full rank and its image spans the nullspace of C , i.e., (7) holds.*

Proof. Recall Sylvester's matrix rank inequality, which states $\text{rank}(M_1M_2) \geq \text{rank } M_1 + \text{rank } M_2 - n$ for any two matrices $M_1, M_2 \in \mathbb{R}^{n \times n}$. It holds that $\text{rank } R^{(\nu)} = n^{(pw)} - 1$ and we have $\text{rank } B^{(\nu)} \geq \text{rank } B^{(\nu-1)} - 1 \geq \text{rank } B^{(0)} - \nu = n^{(pw)} - \nu$. Since B consists of the non-vanishing columns of $B^{(N)}$, we know $\text{rank } B = \text{rank } B^{(N)} \geq n^{(pw)} - N$. By construction, in each elimination step one column $B^{(\nu-1)}$ is eliminated, at least N columns of $B^{(N)}$ vanish and thus

$$\text{rank } B = \text{rank } B^{(N)} = n^{(pw)} - N \quad \text{and} \quad B \in \mathbb{R}^{n^{(pw)} \times (n^{(pw)} - N)},$$

which already shows that B has full rank.

Since $CB^{(N)} = 0$ and B is composed of the non-zero columns of $B^{(N)}$, we have

$$\text{image } B = \text{image } B^{(N)} \subseteq \text{nullspace } C.$$

Now, we show that these are equal by showing $\text{rank } B^{(N)} + \text{rank } C \geq n^{(pw)}$. Using

$$CB^{(\nu)} = \left(I - \frac{1}{\underline{e}_{m_\nu}^\top CB^{(\nu-1)} \underline{e}_{n_\nu}} CB^{(\nu-1)} \underline{e}_{n_\nu} \underline{e}_{m_\nu}^\top \right) CB^{(\nu-1)},$$

where m_ν and n_ν are as chosen in iterate ν in the algorithm, we know $\text{nullspace}(CB^{(\nu-1)}) \subseteq \text{nullspace}(CB^{(\nu)})$ and $\underline{e}_{n_\nu} \in \text{nullspace}(CB^{(\nu)})$. Since (10) guarantees that $\underline{e}_{m_\nu}^\top CB^{(\nu-1)} \underline{e}_{n_\nu} \neq 0$, we know that $\underline{e}_{n_\nu} \notin \text{nullspace}(CB^{(\nu-1)})$. Thus, $\text{rank } CB^{(\nu)} \leq \text{rank } CB^{(\nu-1)} - 1 \leq \text{rank } C - \nu$. By further using $CB^{(N)} = 0$, we have $\text{rank } C \geq N$. Since we have already shown $\text{rank } B^{(N)} \geq n^{(pw)} - N$, this shows $\text{rank } B^{(N)} + \text{rank } C \geq n^{(pw)}$ and thus finishes the proof. \square

Lemma 4.2. *The returned matrix B has only non-negative coefficients, i.e., (9) holds.*

Proof. (10) and the definition of $R^{(\nu)}$ guarantee that all its coefficients are non-negative. This result carries over to $B^{(N)} = R^{(1)} \dots R^{(N)}$ and B being composed of the non-vanishing columns of $B^{(N)}$. \square

Lemma 4.3. *The returned matrix B represents a partition of unity, i.e., (8) holds.*

Proof. Let $\underline{e} = (1, \dots, 1)^\top$. First, we show that

$$CB^{(\nu)}\underline{e} = 0 \quad \text{for all } \nu = 0, \dots, N. \quad (12)$$

by induction. Since the row-sum of the embedding matrices $E^{(k,\ell)}$ is 1, we know by construction (6) that $C\underline{e} = 0$, i.e., (12) for $\nu = 0$. Assuming $CB^{(\nu-1)}\underline{e} = 0$ for some ν , we have

$$CB^{(\nu)}\underline{e} = CB^{(\nu-1)}\underline{e} - \frac{1}{\underline{e}_{m_\nu}^\top CB^{(\nu-1)}\underline{e}_{n_\nu}} CB^{(\nu-1)}\underline{e}_{n_\nu} \underline{e}_{m_\nu}^\top CB^{(\nu-1)}\underline{e} = 0,$$

i.e., (12). Using (12) and (11), we know that $R^{(\nu)}\underline{e} = \underline{e}$. By induction, this shows $B^{(N)}\underline{e} = R^{(N)} \dots R^{(1)}\underline{e} = \underline{e}$. Since B consists of the non-zero columns of $B^{(N)}$, the desired result immediately follows. \square

Now, we give a result that allows us to show that in each step of the Algorithm, there is at least one row m_ν such that $\mathcal{F}_{m_\nu}(CB^{(\nu-1)})$ is not empty.

Lemma 4.4. *For any $\mathcal{M} \subseteq \{1, \dots, M\}$ with $|\mathcal{M}| \leq \text{rank } C$, there are $(\eta_m)_{m \in \mathcal{M}}$ such that*

$$\begin{aligned} \eta_m &\in \mathcal{F}_m(C) && \text{for all } m \in \mathcal{M} \\ \eta_m &\neq \eta_{\tilde{m}} && \text{for all } m \neq \tilde{m}, m, \tilde{m} \in \mathcal{M}. \end{aligned} \quad (13)$$

Proof. First, we observe that the construction (6) guarantees that each row m of C has exactly one positive entry p_m , i.e., we have $C_{m,p_m} > 0$, and thus $p_m \in \mathcal{F}_m(C)$. For a constraint that is not related to corner or T-junction, this is depicted in Figure 2 (a). For this case, we choose $\eta_m := p_m$.

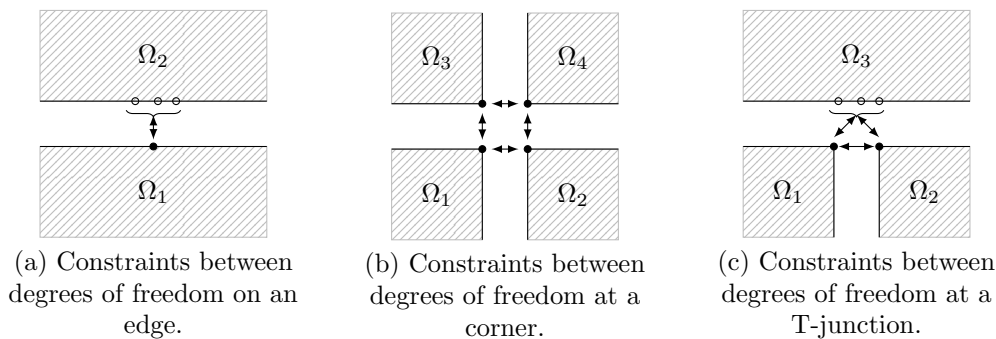


Figure 2: Schematic representation of constraints

Since the matrix C is constructed on an edge-by-edge basis, it is possible that there is more than one positive coefficient in a column of C if the column corresponds to a degree of freedom that is associated to more than one edge, i.e., a degree of freedom associated to the corner of a patch. These cases are depicted in Figure 2 (b) and (c), where η_m has to be chosen more carefully in order to guarantee (13).

Now, consider the case of regular corners (cf. Figure 2 (b)).

Since B-splines interpolate at the boundary, the corresponding rows m of the matrix C contain exactly one positive and one negative coefficient, i.e., there is a p_m and a n_m such that $C_{m,n_m} < 0$ and $C_{m,p_m} > 0$ and $\mathcal{F}_m(C) = \{n_m, p_m\}$. For these constraints, one can choose either $\eta_m = n_m$ or $\eta_m = p_m$; in order to guarantee (13), we choose a cyclic version.

Now consider the case of T-junctions, where we have two kinds of constraints (cf. Figure 2 (c)). Two constraints enforce that each of the local corner values agrees with the corresponding function value on the edge, while the remaining constraint guarantee that the two corner values agree. (If more than 3 patches would meet at a T-junction, there would be accordingly more constraints that guarantee that two corner values agree.) Again, the constraints involving two corner values correspond to a row m of C with exactly one positive and one negative coefficient (where η_m could be either of them). For the other two rows we only know that there is exactly one positive coefficient (where η_m could only be the positive one).

Here, it is in general not possible to choose η_m in a cyclic way as for the regular corners. Since one of the constraints at the T-junction is redundant (this is also valid for a regular corner, but there we did not need this argument), the set \mathcal{M} does not contain all of these constraints. By removing one of the constraints, one can again choose $\eta_m \in \mathcal{F}_m(C)$ with (13). \square

Lemma 4.5. *In all steps of the iteration, it is possible to find some index such that (10) holds.*

Proof. We make a proof by contradiction. Let $C^{(\nu)} := CB^{(\nu)}$.

Assume that after performing ν^* steps, we have $C^{(\nu^*)} \neq 0$ and there is no row such that (10) holds.

We observe that the ordering of the rows of C does not have a direct effect to the algorithm; so we assume that the first ν^* rows correspond to the rows eliminated in the first ν^* steps of the algorithm, i.e., $m_1 = 1, m_2 = 2, \dots, m_{\nu^*} = \nu^*$. Since $C^{(\nu^*)} \neq 0$, there is at least one row that does not vanish; without loss of generality, we assume that the row $\nu^* + 1$ does not vanish. Consequently, we know for all $\nu = 0, \dots, \nu^*$ that (a) the first ν rows of $C^{(\nu)}$ vanish and (b) conversely, because of (10), the row $\nu + 1$ of $C^{(\nu)}$ does not vanish. From the combination of items (a) and (b), we know that the first $\nu^* + 1$ rows of C are linear independent.

Lemma 4.4 with $\mathcal{M} := \{1, 2, \dots, \nu^* + 1\}$ gives the following statement for $\nu = 0$:

$$\text{There are } \eta_{\nu+1}^{(\nu)} \neq \dots \neq \eta_{\nu^*+1}^{(\nu)} \text{ such that } \eta_m^{(\nu)} \in \mathcal{F}_m(C^{(\nu)}) \text{ for all } m = \nu, \dots, \nu^* + 1. \quad (14)$$

If we know this statement for $\nu = \nu^*$, we know that Algorithm 4.1 can proceed after the step ν^* , which is a contradiction to the assumption that this was not the case.

We show (14) by induction; we assume that it holds for some $\nu - 1$. In the ν -th step of the algorithm, we choose $m_\nu = \nu$ (as assumed above) and some $n_\nu \in \mathcal{F}_{m_\nu}(C^{(\nu-1)})$. Now, we have to consider two cases.

The *first case* is $n_\nu = \eta_\nu^{(\nu-1)}$. (We know from (14) that $\eta_\nu^{(\nu-1)} \in \mathcal{F}_{m_\nu}(C^{(\nu-1)})$, i.e., that it is a feasible choice.) Now consider any $i \in \{\nu + 1, \dots, \nu^* + 1\}$. Without loss of generality, assume that $C_{i,\eta_i^{(\nu-1)}}^{(\nu-1)} > 0$ (the case < 0 is analogous). Using $n_\nu = \eta_\nu^{(\nu-1)} \neq \eta_i^{(\nu-1)}$, we have

$$C_{i,j}^{(\nu)} = \underbrace{C_{i,j}^{(\nu-1)}}_{\leq 0} - \frac{C_{\nu,j}^{(\nu-1)}}{C_{\nu,n_\nu}^{(\nu-1)}} \underbrace{C_{i,n_\nu}^{(\nu-1)}}_{\leq 0} \leq 0 \text{ for all } j \notin \{n_\nu, \eta_i^{(\nu-1)}\} \quad \text{and} \quad C_{i,n_\nu}^{(\nu)} = 0.$$

This means that $j = \eta_i^{(\nu-1)}$ is the only candidate to obtain $C_{i,j}^{(\nu)} > 0$. Since the i -th row does not vanish and the row-sum is zero, we know that $C_{i,\eta_i^{(\nu-1)}}^{(\nu)} > 0$ and thus $\eta_i^{(\nu)} := \eta_i^{(\nu-1)} \in \mathcal{F}_\nu(C^{(\nu-1)})$. Since this holds for all i , we know (14) for ν in the first case.

Now, consider the *second case*, i.e., $n_\nu \neq \eta_{\nu-1}^{(\nu-1)}$. Since the set \mathcal{F}_ν can have at most two members and using (14) and (10), we know that $\mathcal{F}_\nu(C^{(\nu-1)}) = \{n_\nu, \eta_\nu^{(\nu-1)}\}$. In this case, $C_{\nu,j}^{(\nu-1)} = 0$ for $j \notin \{n_\nu, \eta_\nu^{(\nu-1)}\}$. Since the row sum of $C^{(\nu-1)}$ is known to be zero, we have $C_{\nu,n_\nu}^{(\nu-1)} = -C_{\nu,\eta_\nu^{(\nu-1)}}^{(\nu-1)}$. Thus, we have

$$C_{i,j}^{(\nu)} = \begin{cases} 0 & \text{if } j = n_\nu \\ C_{i,\eta_\nu^{(\nu-1)}}^{(\nu-1)} + C_{i,n_\nu}^{(\nu-1)} & \text{if } j = \eta_\nu^{(\nu-1)} \\ C_{i,j}^{(\nu-1)} & \text{otherwise.} \end{cases}$$

So, if $\eta_i^{(\nu-1)} \neq n_\nu$, then $\eta_i^{(\nu)} := \eta_j^{(\nu-1)} \in \mathcal{F}_i(C^{(\nu)})$ with the same arguments as above. Conversely, if $\eta_i^{(\nu-1)} = n_\nu$, then $\eta_i^{(\nu)} := \eta_\nu^{(\nu-1)} \in \mathcal{F}_i(C^{(\nu)})$. Since this holds for all i , we know (14) for ν also in the second case.

By induction, we obtain (14) for $\nu^* + 1$. This is in contradiction to the assumption that the algorithm cannot proceed after step ν^* . This finishes the proof. \square

5 Approximation error estimates

In this section, we investigate the approximation power of the multi-patch spline space V_h , as introduced in (1). Specifically, give an approximation error estimate in terms of the local mesh sizes, while also considering the patch-wise prescribed regularity of the solution. We assume $u \in H^{1+q_k}(\Omega_k)$, where $q_k \in (0, p]$ is an appropriate regularity parameter. If q_k is an integer, the associated norm $\|u\|_{H^{1+q_k}(\Omega_k)}$ is the standard norm based on the L^2 -norms of all partial derivatives of total order $\leq 1 + q_k$. If q_k is not an integer, we assume $\|u\|_{H^{1+q_k}(\Omega_k)}$ to be as defined by real Hilbert space interpolation of $\|u\|_{H^{1+\lfloor q_k \rfloor}(\Omega_k)}$ and $\|u\|_{H^{1+\lceil q_k \rceil}(\Omega_k)}$ via the K-method, see [1]. Certainly, other ways of defining the norm lead to the same space, however only with *equivalent* norms. For simplicity, we collect the local regularities to a vector $q = (q_1, \dots, q_K)$ and write $\mathcal{H}^{1+q}(\Omega) := \{u \in H^1(\Omega) : u|_{\Omega_k} \in H^{1+q_k}(\Omega_k)\}$. Additionally we assume uniform grids for all patches.

Assumption 5.1. For each patch Ω_k , there is a specific grid size \widehat{h}_k such that the corresponding knot vectors are uniform, i.e., of the form $\Xi^{(k,1)} = \Xi^{(k,2)} = (0, \dots, 0, \widehat{h}_k, 2\widehat{h}_k, \dots, 1 - \widehat{h}_k, 1, \dots, 1)$.

Within this section, we give a proof for the following two main theorems.

Theorem 5.1. *Assume that the Assumptions 2.1, 3.1, 3.3, 3.4, 3.2 and 5.1 hold. Then, there is a constant $c > 0$ that only depends on the constant C_G from Assumption 2.1 such that for any $q = (q_1, \dots, q_K)$ with $q_k \in [1, p]$, the following approximation error estimate holds:*

$$\inf_{u_h \in V_h} \|u - u_h\|_{H^1(\Omega)}^2 \leq c \sum_{k=1}^K h_k^{2q_k} \|u\|_{H^{1+q_k}(\Omega_k)}^2 \quad \text{for all } u \in \mathcal{H}^{1+q}(\Omega).$$

In case of reduced regularity, the estimate weakens slightly and we obtain the following result.

Theorem 5.2. *Assume that the Assumptions 2.1, 3.1, 3.3, 3.4, 3.2 and 5.1 hold. Then, for any $q = (q_1, \dots, q_K)$ with $q_k \in (0, p]$ and any $\varepsilon \in (0, \min_k q_k)$, the following approximation error estimate holds:*

$$\inf_{u_h \in V_h} \|u - u_h\|_{H^1(\Omega)}^2 \leq c_\varepsilon p \max_\ell \left(1 + \log \frac{H_\ell}{h_\ell} + \log p\right) |\mathbb{V}(\Omega_\ell)| \sum_{k=1}^K h_k^{2(q_k - \varepsilon)} \|u\|_{H^{1+q_k}(\Omega_k)}^2,$$

where c_ε is a constant that only depends on ε and the constant C_G from Assumption 2.1 and $|\mathbb{V}(\Omega_k)|$ is the number of vertices (T -junctions and corners) located on the boundary of the patch Ω_k .

Throughout this section, we write $a \lesssim b$ if there is a constant $c > 0$ that only depends on the constant C_G from Assumption 2.1 such that $a \leq cb$. If $a \lesssim b$ and $b \lesssim a$, we write $a \approx b$.

We derive the estimate from Theorems 5.1 and 5.2 constructively in three steps. First, we consider local projections on each of the patches and present error estimates for those. These local projections can be interpreted as a global approximation by a function that is typically discontinuous between patches. Then, we employ corrections guaranteeing continuity; this is done in two steps: first for each of the vertices, then for the edges between any two patches.

Remark. We have introduced Assumption 5.1 such that we can write down the mentioned correction terms more easily. An extension to the case of non-uniform grids is, although very technical, a straight-forward extension. Since we use results from [19] to prove that theorem, the estimate from Theorem 5.2 would then depend on the quasi-uniformity of the grid within each patch, i.e., on $\max_k \hat{h}_k / \hat{h}_{k, \min}$.

Remark. Note that the constants c and c_ε are independent of the local grid sizes h_k , the diameters of the patches H_k , the spline degree p , and the smoothness of the B-splines.

5.1 Geometric setup

In order to derive the theory, we need some more notation. We already know that the overall computational domain Ω is composed of K disjointed patches Ω_k , each being the image of a parameterization, i.e., $\Omega_k = G_k(\hat{\Omega})$, where $\hat{\Omega} = (0, 1)^2$. The interfaces between these patches are edges and vertices. Each patch Ω_k has four corners $\{G_k(\hat{\mathbf{x}}) : \hat{\mathbf{x}} \in \{0, 1\}^2\}$. We call the points in the interior of Ω that are the corner of a patch *vertex* and enumerate all vertices, i.e., we have

$$\{\mathbf{x}_1, \dots, \mathbf{x}_M\} = \{G_k(\hat{\mathbf{x}}_m^{(k)}) : \hat{\mathbf{x}}_m^{(k)} \in \{0, 1\}^2, G_k(\hat{\mathbf{x}}_m^{(k)}) \notin \partial\Omega\} \quad \text{with } \mathbf{x}_m \neq \mathbf{x}_n \text{ for } m \neq n.$$

It can happen that a vertex is located on the edge of an adjacent patch, rather than on one of its corners; we call these vertices *T-junctions*. Vertices that are the corner of all adjacent patches are called *corner vertices*; in the example of Figure 3, \mathbf{x}_1 is a T-junction and all other vertices are a corner vertices. Analogously, we consider the edges between patches. Let

$$\{\Gamma_1, \dots, \Gamma_J\} = \{\partial\Omega_k \cap \partial\Omega_\ell : (k, \ell) \text{ arbitrarily with } |\partial\Omega_k \cap \partial\Omega_\ell| > 0\} \quad \text{with } \Gamma_i \neq \Gamma_j \text{ for } i \neq j.$$

be the set of distinct edges. Note that the definition does not include segments on the boundary. An edge is the segment of an interface between two patches that is enclosed between two vertices.

We denote by $\mathbb{C}(\Omega_k)$ the indices of the vertices \mathbf{x}_m that are located on the corners of Ω_k and by $\mathbb{T}(\Omega_k)$ the indices of the vertices that are located on the remainder of $\partial\Omega_k$. $\mathbb{V}(\Omega_k) := \mathbb{T}(\Omega_k) \cup \mathbb{C}(\Omega_k)$

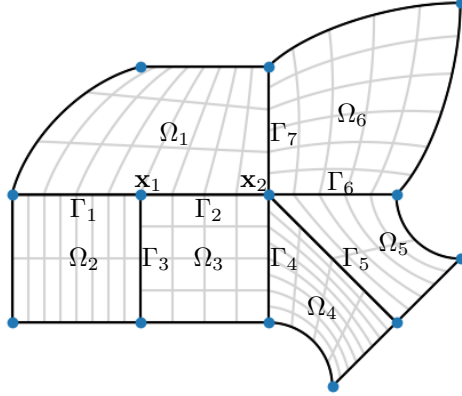


Figure 3: Example with 5 patches Ω_k , 7 edges Γ_i , T-junction \mathbf{x}_1 and corner vertex \mathbf{x}_2 .

and $\mathbb{E}(\Omega_k)$ denote the indices of the vertices and edges, respectively, that are located on $\partial\Omega_k$. Analogously, $\mathbb{V}(\Gamma_i)$ refers to the 2 vertices that enclose the edge Γ_i . Conversely, we denote by $\mathbb{P}(\mathbf{x}_m) := \{k : m \in \mathbb{V}(\Omega_k)\}$, $\mathbb{P}(\Gamma_i) := \{k : i \in \mathbb{E}(\Omega_k)\}$, $\mathbb{E}(\mathbf{x}_m) := \{i : m \in \mathbb{V}(\Gamma_i)\}$ the patches and edges that are adjacent to the vertex \mathbf{x}_m or the edge Γ_i .

Following this pattern, $\mathbb{V} := \bigcup_{k=1}^K \mathbb{V}(\Omega_k)$, $\mathbb{T} := \bigcup_{k=1}^K \mathbb{T}(\Omega_k)$, $\mathbb{C} := \mathbb{V} \setminus \mathbb{T}$ and $\mathbb{E} := \bigcup_{k=1}^K \mathbb{E}(\Omega_k)$ refer to all vertices, all T-junctions, all corner vertices and all edges, respectively. In the example of Figure 3, we have $\mathbf{x}_1 \in \mathbb{T}$ since it is a T-junction and $\mathbf{x}_1 \in \mathbb{T}(\Omega_1)$ since \mathbf{x}_1 is not located on a corner of Ω_1 , but $\mathbf{x}_1 \in \mathbb{C}(\Omega_2)$ and $\mathbf{x}_1 \notin \mathbb{T}(\Omega_2)$ since \mathbf{x}_1 is located on a corner of Ω_2 .

5.2 Patch-local quasi-interpolation

In this section, we want to recall some standard quasi-interpolation error estimates, which we use for a patch-local construction of a quasi-interpolation operator.

The error estimates are based on the H^1 -orthogonal projector for functions in one dimension. The projector $\widehat{\Pi}_h^{(k,\delta)} : H^1(0,1) \rightarrow \widehat{V}_h^{(k,\delta)}$ is defined via the orthogonality property $(\widehat{u} - \widehat{\Pi}_h^{(k,\delta)}\widehat{u}, \widehat{v}_h)_{H_D^1(0,1)} = 0$ for all $\widehat{v}_h \in \widehat{V}_h^{(k,\delta)}$, where

$$(\widehat{u}, \widehat{v})_{H_D^1(0,1)} := \int_0^1 \widehat{u}(x)\widehat{v}(x) dx + \widehat{u}(0)\widehat{v}(0).$$

Besides being H^1 -orthogonal, the constant values are chosen such that $\widehat{\Pi}_h^{(k,\delta)}\widehat{u}(0) = \widehat{u}(0)$. In [21], it was shown that also $\widehat{\Pi}_h^{(k,\delta)}\widehat{u}(1) = \widehat{u}(1)$ holds. [17] gives the following estimates:

$$\|\widehat{u} - \widehat{\Pi}_h^{(k,\delta)}\widehat{u}\|_{L^2(0,1)} \leq \left(\frac{\widehat{h}_k}{\pi}\right)^{1+q_k} |\widehat{u}|_{H^{1+q_k}(0,1)} \quad \text{and} \quad |\widehat{u} - \widehat{\Pi}_h^{(k,\delta)}\widehat{u}|_{H^1(0,1)} \leq \left(\frac{\widehat{h}_k}{\pi}\right)^{q_k} |\widehat{u}|_{H^{1+q_k}(0,1)} \quad (15)$$

for $q_k \in \{0, \dots, p\}$.

There are several possibilities to extend this to functions defined on $\widehat{\Omega} = (0,1)^2$. If $\widehat{u} \in H^2(\widehat{\Omega})$, the tensor product of the projectors $\widehat{\Pi}_h^{(k,1)}$ and $\widehat{\Pi}_h^{(k,2)}$ is well-defined and maps into \widehat{V}_h , see [21] for details. The following lemma collects the corresponding results.

Lemma 5.1. *There is a projector $\widehat{\Pi}_h^{(k)} : H^2(\widehat{\Omega}) \rightarrow \widehat{V}_h^{(k)}$ that satisfies the following statements:*

- $\widehat{\Pi}_h^{(k)}$ interpolates at the corners of $\widehat{\Omega}$, i.e.,

$$(\widehat{\Pi}_h^{(k)} \widehat{u})(\widehat{\mathbf{x}}) = \widehat{u}(\widehat{\mathbf{x}}) \quad \text{for all } \widehat{\mathbf{x}} \in \{0, 1\}^2 \text{ and } \widehat{u} \in H^2(\widehat{\Omega}). \quad (16)$$

- Its restriction to an edge is equal to a projection on that edge; particularly,

$$|\widehat{u} - \widehat{\Pi}_h^{(k)} \widehat{u}|_{H^1(\widehat{\Gamma})} = \inf_{\widehat{v}_h \in \widehat{V}_h^{(k)}} |\widehat{u} - \widehat{v}_h|_{H^1(\widehat{\Gamma})}, \quad (17)$$

and satisfies the approximation error estimate

$$\|\widehat{u} - \widehat{\Pi}_h^{(k)} \widehat{u}\|_{L^2(\widehat{\Gamma})} \lesssim h_k |\widehat{u} - \widehat{\Pi}_h^{(k)} \widehat{u}|_{H^1(\widehat{\Gamma})} \quad (18)$$

for all sides $\widehat{\Gamma} \in \{\{0\} \times (0, 1), \{1\} \times (0, 1), (0, 1) \times \{0\}, (0, 1) \times \{1\}\}$ and all $\widehat{u} \in H^2(\widehat{\Omega})$.

- It minimizes the error in the H^1 -seminorm

$$|\widehat{u} - \widehat{\Pi}_h^{(k)} \widehat{u}|_{H^1(\widehat{\Omega})} = \inf_{\widehat{v}_h \in \widehat{V}_h^{(k)}} |\widehat{u} - \widehat{v}_h|_{H^1(\widehat{\Omega})}$$

and satisfies the approximation error estimates

$$\|\widehat{u} - \widehat{\Pi}_h^{(k)} \widehat{u}\|_{L^2(\widehat{\Omega})} \lesssim \widehat{h}_k^{1+q_k} |\widehat{u}|_{H^{1+q_k}(\widehat{\Omega})}, \quad (19)$$

$$|\widehat{u} - \widehat{\Pi}_h^{(k)} \widehat{u}|_{H^1(\widehat{\Omega})} \lesssim \widehat{h}_k^{q_k} |\widehat{u}|_{H^{1+q_k}(\widehat{\Omega})}, \quad (20)$$

$$\|\partial_{\widehat{x}, \widehat{y}}(\widehat{u} - \widehat{\Pi}_h^{(k)} \widehat{u})\|_{L^2(\widehat{\Omega})} \lesssim \widehat{h}_k^{-1+q_k} |\widehat{u}|_{H^{1+q_k}(\widehat{\Omega})} \quad (21)$$

for all $\widehat{u} \in H^{1+q_k}(\widehat{\Omega})$.

The statements (16) and (17) are direct consequence of [21, Theorem 3.4]. For the case $q_k = 1$ [21, Theorem 3.3] gives (20); the estimates (19) and (21) follow analogously from [21, Theorems 3.1 and 3.2]. (18) directly follows from (15). Using the approximation error estimates from [17], we can immediately extend the result to arbitrary $q_k \in \{1, \dots, p\}$. The estimates (19) and (20) can be carried over to the physical patch Ω_k using the following lemma.

Lemma 5.2. *For all patches Ω_k and all $u \in H^r(\Omega_k)$ with $r = 1, \dots, r_k + 1$, the following estimates hold:*

$$\|u\|_{L^2(\Omega_k)}^2 \approx H_k^2 \|u \circ G_k\|_{L^2(\widehat{\Omega})}^2 \quad \text{and} \quad \sum_{\ell=1}^r |u|_{H^\ell(\Omega_k)}^2 \approx \sum_{\ell=1}^r H_k^{2-2\ell} |u \circ G_k|_{H^\ell(\widehat{\Omega})}^2.$$

Proof. These results follow from Assumption 2.1 and standard chain and substitution rules. \square

We define $\Pi_h^{(k)}$ using the pull-back principle:

$$\Pi_h^{(k)} u := (\widehat{\Pi}_h^{(k)}(u \circ G_k)) \circ G_k^{-1}.$$

Using this definition, Lemma 5.2, (19), (20), $H_k \leq \text{diam } \Omega \approx 1$ and $h_k = \widehat{h}_k H_k$, we have

$$\|u - \Pi_h^{(k)} u\|_{L^2(\Omega_k)} \lesssim H_k \|\widehat{u} - \widehat{\Pi}_h^{(k)} \widehat{u}\|_{L^2(\widehat{\Omega})} \leq H_k \left(\frac{\widehat{h}_k}{\pi}\right)^{1+q_k} |\widehat{u}|_{H^{1+q_k}(\widehat{\Omega})} \lesssim \left(\frac{h_k}{\pi}\right)^{1+q_k} \|u\|_{H^{1+q_k}(\Omega_k)}, \quad (22)$$

$$\|u - \Pi_h^{(k)} u\|_{H^1(\Omega_k)} \lesssim \|\widehat{u} - \widehat{\Pi}_h^{(k)} \widehat{u}\|_{H^1(\widehat{\Omega})} \leq \left(\frac{\widehat{h}_k}{\pi}\right)^{q_k} |\widehat{u}|_{H^{1+q_k}(\widehat{\Omega})} \lesssim \left(\frac{h_k}{\pi}\right)^{q_k} \|u\|_{H^{1+q_k}(\Omega_k)}, \quad (23)$$

$$\widehat{h}_k^2 \|\partial_{\widehat{x}, \widehat{y}}(\widehat{u} - \widehat{\Pi}_h^{(k)} \widehat{u})\|_{L^2(\widehat{\Omega})} \leq \left(\frac{\widehat{h}_k}{\pi}\right)^{q_k} |\widehat{u}|_{H^{1+q_k}(\widehat{\Omega})} \lesssim \left(\frac{h_k}{\pi}\right)^{q_k} \|u\|_{H^{1+q_k}(\Omega_k)} \quad (24)$$

for all $u \in H^{1+q_k}(\Omega_k)$ with pull-back $\widehat{u} := u \circ G_k$. If q_k is not an integer, the same estimates can be derived both for $\lfloor q_k \rfloor$ and $\lceil q_k \rceil$; the desired result is then obtained by the Hilbert space interpolation theorem, see [1, Theorem 7.23].

Remark. The result from [21] is based on [22], which holds for uniform grids (which we have assumed also in this paper). An extension to quasi-uniform grids is possible by using the results from [17].

Remark. If there were no T-junctions and if the trace spaces on all edges would match, i.e.,

$$V_h^{(k)}|_{\Gamma_i} = V_h^{(\ell)}|_{\Gamma_i}$$

for all edges Γ_i with adjacent patches Ω_k and Ω_ℓ ($\{k, \ell\} = \mathbb{P}(\Gamma_i)$), then (16) and (17) would guarantee that a patch-wise defined function u_h with $u_h|_{\Omega_k} := \Pi_k(u|_{\Omega_k})$ would be continuous and thus satisfy $u_h \in V_h$. As a consequence, Theorem 5.1 would directly follow from (22) and (23).

Since we only require Assumption 3.3, we have to construct a correction in order to guarantee the continuity of u_h , which is required to obtain $u_h \in V_h \subset H^1(\Omega)$.

5.3 Traces for edges and vertices

To achieve comparable quasi-interpolation error estimates within lower-dimensional manifolds (edges in this case), it is imperative to establish the subsequent trace inequalities. Using the fundamental theorem of calculus and Young's inequality, we immediately obtain

$$|u(x)|^2 \leq \|u\|_{L^2(0,1)}^2 + \|u\|_{L^2(0,1)} |u|_{H^1(0,1)} \leq 2\eta^{-1} \|u\|_{L^2(0,1)}^2 + \eta |u|_{H^1(0,1)}^2$$

for all $u \in H^1(0,1)$, all $x \in [0,1]$ and all $\eta \in (0,1]$. By building corresponding tensor products, we immediately obtain as follows.

Lemma 5.3. *For all $\widehat{h} \in (0,1]$, it holds that*

$$\begin{aligned} \sum_{i \in \mathbb{E}(\Omega_k)} \|\widehat{u}\|_{L^2(\widehat{\Gamma}_i^{(k)})}^2 &\lesssim \widehat{h}^{-1} \|\widehat{u}\|_{L^2(\widehat{\Omega})}^2 + \widehat{h} |\widehat{u}|_{H^1(\widehat{\Omega})}^2 \quad \text{for all } \widehat{u} \in H^1(\widehat{\Omega}), \\ \sum_{i \in \mathbb{E}(\Omega_k)} |\widehat{u}|_{H^1(\widehat{\Gamma}_i^{(k)})}^2 &\lesssim \widehat{h}^{-1} |\widehat{u}|_{H^1(\widehat{\Omega})}^2 + \widehat{h} \|\partial_{\widehat{x}, \widehat{y}} \widehat{u}\|_{L^2(\widehat{\Omega})}^2 \quad \text{for all } \widehat{u} \in H^2(\widehat{\Omega}), \end{aligned}$$

where $\widehat{\Gamma}_i^{(k)} := G_k^{-1}(\Gamma_i)$ is the pull-back of Γ_i .

Proof. Let $\widehat{\Gamma}$ be one of the four sides of $\widehat{\Omega}$. Without loss of generality we assume $\widehat{\Gamma} = (0, 1) \times \{0\}$.

By applying the fundamental theorem of calculus to \widehat{u}^2 and using Young's inequality, we immediately obtain

$$\|\widehat{u}\|_{L^2(\widehat{\Gamma})}^2 \lesssim \|\widehat{u}\|_{L^2(\widehat{\Omega})}^2 + \|\widehat{u}\|_{L^2(\widehat{\Omega})} \|\partial_{\widehat{y}} \widehat{u}\|_{L^2(\widehat{\Omega})} \lesssim \widehat{h}^{-1} \|\widehat{u}\|_{L^2(\widehat{\Omega})}^2 + \widehat{h} |\widehat{u}|_{H^1(\widehat{\Omega})}^2. \quad (25)$$

By taking the sum over all four sides, we obtain a corresponding result for $\partial\widehat{\Omega}$. The first statement of the lemma follows since $\bigcup_{i \in \mathbb{E}(\Omega_k)} \widehat{\Gamma}_i^{(k)} \subseteq \partial\widehat{\Omega}$. (We obtain equality if $\partial\Omega_k$ does not contribute to the (Dirichlet) boundary $\partial\Omega$.) The second estimate is obtained analogously by substituting the derivative of \widehat{u} in direction of $\widehat{\Gamma}$ into (25). \square

The relation between the norm on Γ_i and on its pull-back $\widehat{\Gamma}_i^{(k)}$ is provided by the following lemma.

Lemma 5.4. *For all patches Ω_k with adjacent edge Γ_i ($i \in \mathbb{E}(\Omega_k)$) and pre-image $\widehat{\Gamma}_i^{(k)} = G_k^{-1}(\Gamma_i)$, the following estimates hold:*

$$\|u\|_{L^2(\Gamma_i)}^2 \approx H_k \|u \circ G_k\|_{L^2(\widehat{\Gamma}_i^{(k)})}^2 \quad \text{and} \quad |u|_{H^1(\Gamma_i)}^2 \approx H_k^{-1} |u \circ G_k|_{H^1(\widehat{\Gamma}_i^{(k)})}^2,$$

for all $u \in L^2(\Gamma_i)$ or $u \in H^1(\Gamma_i)$, respectively.

Proof. Analogously to Lemma 5.2, this result follows using standard chain and substitution rules. \square

With similar arguments, we obtain the following trace theorem.

Lemma 5.5. *For all patches Ω_k with adjacent edge Γ_i ($i \in \mathbb{E}(\Omega_k)$) and pre-image $\widehat{\Gamma}_i^{(k)} = G_k^{-1}(\Gamma_i)$, the following estimates hold:*

$$\begin{aligned} \sum_{m \in \mathbb{V}(\Gamma_i)} |\widehat{u}(\widehat{\mathbf{x}}_m^{(k)})|^2 &\lesssim \widehat{h}_k^{-1} \|\widehat{u}\|_{L^2(\widehat{\Gamma}_i^{(k)})}^2 + \widehat{h}_k |\widehat{u}|_{H^1(\widehat{\Gamma}_i^{(k)})}^2 \quad \text{for all } \widehat{u} \in H^1(\widehat{\Gamma}_i^{(k)}) \\ \sum_{m \in \mathbb{V}(\Omega_k)} |\widehat{u}(\widehat{\mathbf{x}}_m^{(k)})|^2 &\lesssim \widehat{h}_k^{-2} \|\widehat{u}\|_{L^2(\widehat{\Omega})}^2 + |\widehat{u}|_{H^1(\widehat{\Omega})}^2 + \widehat{h}_k^2 \|\partial_{\widehat{x}, \widehat{y}} \widehat{u}\|_{L^2(\widehat{\Omega})}^2 \quad \text{for all } \widehat{u} \in H^2(\widehat{\Omega}), \end{aligned}$$

where $\widehat{\mathbf{x}}_m^{(k)} := G_k^{-1}(\mathbf{x}_m)$ is the pull-back of the vertex \mathbf{x}_m .

Proof. Let $m \in \mathbb{V}(\Gamma_i)$. Because of Assumption 3.4, we know that $|\widehat{\Gamma}_i^{(k)}| \geq \widehat{h}_k$ and thus we have using the fundamental theorem of calculus and Young's inequality

$$|\widehat{u}(\widehat{\mathbf{x}}_m^{(k)})|^2 \lesssim \widehat{h}_k^{-1} \|\widehat{u}\|_{L^2(\widehat{\Gamma}_i^{(k)})}^2 + \widehat{h}_k |\widehat{u}|_{H^1(\widehat{\Gamma}_i^{(k)})}^2.$$

Since each edge is only adjacent to two vertices, this gives the first estimate. Analogously to Lemma 5.3, the second estimate follows from the first one. \square

5.4 Extensions for vertices and edges

As we are working with non-conforming grids, it is necessary to modify the standard projections described in earlier sections. For this purpose, we need a function $\psi_\eta \in \widehat{V}_h^{(k, \delta)}$ such that $\psi_\eta(0) = 1$, $\psi_\eta(1) = 0$ and such that its norm is bounded as discussed below. Such functions are given by

$$\psi_\eta(t) := (\max\{1 - t/\eta, 0\})^p$$

if η is a knot in the corresponding mesh. Since we assume that the grids on the parameter domain are uniform (Assumption 5.1), this is guaranteed if $\eta \in (0, 1]$ is an integer multiple of \widehat{h}_k . Straight-forward computations yield as follows.

Lemma 5.6. *For every $\eta \in (0, 1]$, we have $\|\psi_\eta\|_{L^2(0,1)}^2 \approx p^{-1}\eta$ and $|\psi_\eta|_{H^1(0,1)}^2 \approx p\eta^{-1}$.*

From (16), we immediately know that the local approximation agree at corner vertices. However this is not the case for T-junctions, for which we need to introduce additional corrections in order to guarantee continuity. For each T-junction \mathbf{x}_m , let $k(\mathbf{x}_m)$ be the index of the patch $\Omega_{k(\mathbf{x}_m)}$ such that $m \in \mathbb{T}(\Omega_{k(\mathbf{x}_m)})$. In the example depicted in Figure 4, we have $k(\mathbf{x}_1) = 1$. Due to Assumption 3.2, there are two more patches that are adjacent to \mathbf{x}_m , which we call Ω_ℓ and $\Omega_{\ell'}$. The edge between Ω_ℓ and $\Omega_{\ell'}$ is called Γ_i . Let ℓ and ℓ' be such that

$$V_h^{(\ell)}|_{\Gamma_i} \subseteq V_h^{(\ell')}|_{\Gamma_i}. \quad (26)$$

In the example depicted in Figure 4, we have thus $\ell = 3, \ell' = 2$ and $i = 3$.

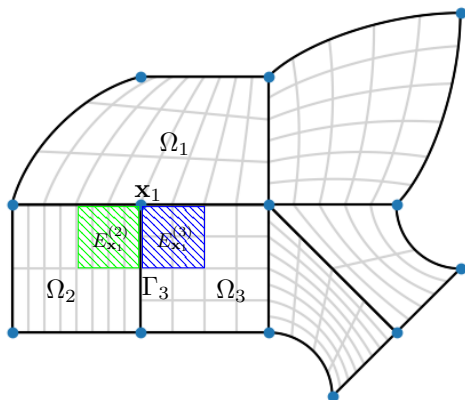


Figure 4: Extensions for the T-junction \mathbf{x}_1 are defined on Ω_2 (support in green) and Ω_3 (support in blue); their depth into the finer patches is adjusted by $h_{k(\mathbf{x}_m)} = h_1$, still aligned with the grids on which they are defined. The extensions agree on the adjacent edge Γ_3 and vanish on all other vertices.

The extension operator $E_{\mathbf{x}_m}^{(\ell)} : \mathbb{R} \rightarrow V_h^{(\ell)}$ is defined by $E_{\mathbf{x}_m}^{(\ell)} s = (\widehat{E}_{\mathbf{x}_m}^{(\ell)} s) \circ G_\ell^{-1}$ with

$$(\widehat{E}_{\mathbf{x}_m}^{(\ell)} s)(\widehat{x}, \widehat{y}) := \psi_\eta(\widehat{x})\psi_\eta(\widehat{y})s \quad \text{and} \quad \eta := \min\{\lceil \frac{ph_{k(\mathbf{x}_m)}}{h_\ell} \rceil, \lfloor \frac{|\widehat{\Gamma}_i^{(\ell)}|}{\widehat{h}_\ell} \rfloor\} \widehat{h}_\ell, \quad (27)$$

where $\lfloor \cdot \rfloor$ and $\lceil \cdot \rceil$ denote the floor and ceiling functions.

The idea is that $\eta \sim ph_{k(\mathbf{x}_m)}H_\ell^{-1}$, but for sure not longer than the length of the pre-image of Γ_i , the edge between Ω_ℓ and $\Omega_{\ell'}$. In order to have $E_{\mathbf{x}_m}^{(\ell)} s \in V_h^{(\ell)}$ or, equivalently, $\widehat{E}_{\mathbf{x}_m}^{(\ell)} s \in \widehat{V}_h^{(\ell)}$, η should correspond to a knot in the corresponding knot vector. Since we have restricted ourselves to the case that the grids on each patch are uniform (Assumption 5.1), this is the case since $\eta \in (0, 1]$ is an integer multiple of \widehat{h}_ℓ .

For the other adjacent patch, the extension operator $E_{\mathbf{x}_m}^{(\ell')} : \mathbb{R} \rightarrow V_h^{(\ell')}$ is defined by $E_{\mathbf{x}_m}^{(\ell')} s = (\widehat{E}_{\mathbf{x}_m}^{(\ell')} s) \circ G_{\ell'}^{-1}$ with

$$(\widehat{E}_{\mathbf{x}_m}^{(\ell')} s)(\widehat{x}, \widehat{y}) := \psi_\eta(\widehat{x}) \psi_\eta(\widehat{y}) s, \quad (28)$$

where η is chosen such that

$$E_{\mathbf{x}_m}^{(\ell')} s|_{\Gamma_i} = E_{\mathbf{x}_m}^{(\ell)} s|_{\Gamma_i}.$$

The statement (26) and Assumption 5.1 guarantee that $E_{\mathbf{x}_m}^{(\ell')} s \in V_h^{(\ell')}$. See Figure 4 for a visualization. The extension operators can be bounded from above as follows.

Lemma 5.7. *Let Ω_k be a patch and the T-junction \mathbf{x}_m be one of its corners ($m \in \mathbb{T} \cap \mathbb{C}(\Omega_k)$). Then, we have*

$$h_{\mathbf{k}(\mathbf{x}_m)}^{-2} \|E_{\mathbf{x}_m}^{(k)} s\|_{L^2(\Omega_k)}^2 + |E_{\mathbf{x}_m}^{(k)} s|_{H^1(\Omega_k)}^2 \lesssim |s|^2 \quad \text{for all } s \in \mathbb{R}.$$

Proof. First, we estimate the size of η from (27) or (28).

Consider the case of (27) first, where $k = \ell$. The estimate $H_\ell \widehat{h}_\ell = h_\ell \leq h_{\mathbf{k}(\mathbf{x}_m)}$ guarantees that $\eta \leq \widehat{h}_\ell + ph_{\mathbf{k}(\mathbf{x}_m)} H_\ell^{-1} \leq 2ph_{\mathbf{k}(\mathbf{x}_m)} H_\ell^{-1}$. Assumption 3.4 guarantees $|\widehat{\Gamma}_i^{(\ell)}| \geq p\widehat{h}_\ell$, thus we have $\eta \geq \min\{ph_{\mathbf{k}(\mathbf{x}_m)} H_\ell^{-1}, \frac{1}{2}|\widehat{\Gamma}_i^{(\ell)}|\}$. Assumption 3.3 guarantees that Γ_i is a full edge of $\Omega_{\ell'}$ and thus Lemma 5.4 and Assumption 3.4 guarantee $|\widehat{\Gamma}_i^{(\ell)}| \approx H_\ell^{-1}|\Gamma_i| \approx H_\ell^{-1}H_{\ell'}|\widehat{\Gamma}_i^{(\ell')}| = H_\ell^{-1}H_{\ell'} \geq H_\ell^{-1}H_{\ell'}|\widehat{\Gamma}_j^{(\ell')}| \approx H_\ell^{-1}|\Gamma_j| \gtrsim ph_{\mathbf{k}(\mathbf{x}_m)} H_\ell^{-1}$, where Γ_j is the edge between $\Omega_{\ell'}$ and $\Omega_{\mathbf{k}(\mathbf{x}_m)}$. Therefore it holds for the case $k = \ell$ that

$$\eta \approx ph_{\mathbf{k}(\mathbf{x}_m)} H_k^{-1}. \quad (29)$$

The other case (28), where $k = \ell'$, follows then directly using Lemma 5.4. Using (29) and Lemma 5.6, we obtain

$$\begin{aligned} \|\widehat{E}_{\mathbf{x}_m}^{(\ell)} s\|_{L^2(\widehat{\Omega})}^2 &= \|\psi_\eta^{(\ell)}\|_{L^2(0,1)}^2 \|\psi_\eta^{(\ell)}\|_{L^2(0,1)}^2 |s|^2 \lesssim p^{-2}\eta^2 |s|^2 \approx H_k^{-2} h_{\mathbf{k}(\mathbf{x}_m)}^2 |s|^2, \\ |\widehat{E}_{\mathbf{x}_m}^{(\ell)} s|_{H^1(\widehat{\Omega})}^2 &= |\psi_\eta^{(\ell)}|_{H^1(0,1)}^2 \|\psi_\eta^{(\ell)}\|_{L^2(0,1)}^2 |s|^2 + \|\psi_\eta^{(\ell)}\|_{L^2(0,1)}^2 |\psi_\eta^{(\ell)}|_{H^1(0,1)}^2 |s|^2 \lesssim |s|^2. \end{aligned}$$

We obtain the desired result using Lemma 5.2. \square

We can also estimate the traces of the extension on the adjacent edges.

Lemma 5.8. *Let Ω_k be a patch, the T-junction \mathbf{x}_m be one of its corners and Γ_i an adjacent edge of Ω_k ($m \in \mathbb{T} \cap \mathbb{C}(\Omega_k) \cap \mathbb{V}(\Gamma_i)$, $i \in \mathbb{E}(\Omega_k)$). Then,*

$$h_{\mathbf{k}(\mathbf{x}_m)}^{-1} \|E_{\mathbf{x}_m}^{(k)} s\|_{L^2(\Gamma_i)}^2 + h_{\mathbf{k}(\mathbf{x}_m)} |E_{\mathbf{x}_m}^{(k)} s|_{H^1(\Gamma_i)}^2 \lesssim |s|^2 \quad \text{for all } s \in \mathbb{R}.$$

Proof. Using Lemma 5.4 and Lemma 5.6 and (29), we have

$$\begin{aligned} h_{\mathbf{k}(\mathbf{x}_m)}^{-1} \|E_{\mathbf{x}_m}^{(k)} s\|_{L^2(\Gamma_i)}^2 + h_{\mathbf{k}(\mathbf{x}_m)} |E_{\mathbf{x}_m}^{(k)} s|_{H^1(\Gamma_i)}^2 &\lesssim h_{\mathbf{k}(\mathbf{x}_m)}^{-1} H_k \|\widehat{E}_{\mathbf{x}_m}^{(k)} s\|_{L^2(\widehat{\Gamma}_i^{(k)})}^2 + h_{\mathbf{k}(\mathbf{x}_m)} H_k^{-1} |\widehat{E}_{\mathbf{x}_m}^{(k)} s|_{H^1(\widehat{\Gamma}_i^{(k)})}^2 \\ &\lesssim (p^{-1} h_{\mathbf{k}(\mathbf{x}_m)}^{-1} H_k \eta + ph_{\mathbf{k}(\mathbf{x}_m)} H_k^{-1} \eta^{-1}) |s|^2 \lesssim |s|^2, \end{aligned}$$

where η is as in (27) or (28), which shows the desired result. \square

Using $\psi_\eta(t) = 0$ for $t \geq \eta$, (27) and Assumption 3.4, we obtain

Lemma 5.9. *Let Ω_k be a patch with corner \mathbf{x}_m , i.e., with $m \in \mathbb{C}(\Omega_k)$. Then*

$$(E_{\mathbf{x}_m}^{(k)}s)(\mathbf{x}_n) = 0 \quad \text{holds for all } n \in \mathbb{V}(\Omega_k).$$

Additionally, we need to ensure continuity across edges. For every edge Γ_i between two patches, let $k(\Gamma_i)$ refer to the adjacent patch with the smaller trace space (if the trace spaces agree, $k(\Gamma_i)$ refers to one of the adjacent patches), i.e., such that

$$V_h^{(k(\Gamma_i))}|_{\Gamma_i} \subseteq V_h^{(\ell)}|_{\Gamma_i} \quad \text{for all } \ell \in \mathbb{P}(\Gamma_i). \quad (30)$$

Remember that $\widehat{\Gamma}_i^{(\ell)} = G_\ell^{-1}(\Gamma_i)$ is the pull-back of Γ_i to the adjacent patch Ω_ℓ with ℓ as above. Using Assumption 3.3, we know that $\widehat{\Gamma}_i^{(\ell)}$ is one of the four sides of $\widehat{\Omega}$; without loss of generality, we assume $\widehat{\Gamma}_i^{(\ell)} = [0, 1] \times \{0\}$, i.e. the interface mapped back to the parameter domain is fixed in the y -component. The extension $E_{\Gamma_i}^{(\ell)} : V_h^{(\ell)}|_{\Gamma_i} \rightarrow \widehat{V}_h^{(\ell)}$ is given by $(E_{\Gamma_i}^{(\ell)}u) \circ G_\ell := \widehat{E}_{\Gamma_i}^{(\ell)}(u \circ G_\ell^{-1})$ with

$$\left(\widehat{E}_{\Gamma_i}^{(\ell)} \widehat{u}\right)(\widehat{x}, \widehat{y}) = \widehat{u}(\widehat{x}, 0)\psi_\eta(\widehat{y}), \quad \text{with } \eta := \left\lceil \frac{ph_{k(\Gamma_i)}}{h_\ell} \right\rceil \widehat{h}_\ell. \quad (31)$$

Analogous to the case of vertex based extensions, we can verify using (30) and Assumption 3.4 that $\eta \in (0, 1]$ and

$$\eta \approx ph_{k(\Gamma_i)}H_\ell^{-1} \quad (32)$$

and that this operator indeed maps into $\widehat{V}_h^{(\ell)}$, see Figure 5 for a visualization.

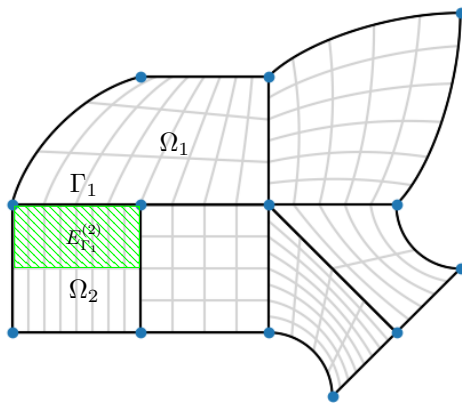


Figure 5: The edge extensions (support in green) extend into the patch with the finer grid, here Ω_2 ; their depth is adjusted to the grid size of the patch with the coarser grid, here Ω_1 , still aligned with the grid on which it is defined. The extension vanishes on all corners and on all other edges.

Using this estimate and Lemma 5.4, we obtain the following lemma.

Lemma 5.10. *Let Ω_k be a patch and Γ_i an adjacent edge ($i \in \mathbb{E}(\Omega_k)$). Then, we have*

$$\|E_{\Gamma_i}^{(k)}u\|_{H^1(\Omega_k)}^2 \lesssim h_{k(\Gamma_i)}^{-1}\|u\|_{L^2(\Gamma_i)}^2 + h_{k(\Gamma_i)}|u|_{H^1(\Gamma_i)}^2 \quad \text{for all } u \in H_0^1(\Gamma_i).$$

Proof. Due to the tensor product structure of the extension operator, we are able to decompose the L^2 -norm and the H^1 -seminorm into their axial components, i.e., we obtain using the chain rule and Lemma 5.6

$$\begin{aligned} |\widehat{E}_{\Gamma_i}^{(k)}(\widehat{u})|_{H^1(\widehat{\Omega})}^2 &= |\widehat{u}|_{H^1(\widehat{\Gamma}_i^{(k)})}^2 \|\psi_\eta\|_{L^2(0,1)}^2 + \|\widehat{u}\|_{L^2(\widehat{\Gamma}_i^{(k)})}^2 |\psi_\eta|_{H^1(0,1)}^2 \lesssim p^{-1}\eta |\widehat{u}|_{H^1(\widehat{\Gamma}_i^{(k)})}^2 + p\eta^{-1} \|\widehat{u}\|_{L^2(\widehat{\Gamma}_i^{(k)})}^2 \\ \|\widehat{E}_{\Gamma_i}^{(k)}(\widehat{u})\|_{L^2(\widehat{\Omega})}^2 &= \|\widehat{u}\|_{L^2(\widehat{\Gamma}_i^{(k)})}^2 \|\psi_\eta\|_{L^2(0,1)}^2 \lesssim p^{-1}\eta \|\widehat{u}\|_{L^2(\widehat{\Gamma}_i^{(k)})}^2, \end{aligned}$$

where η is as in (31). Using (32) and Lemmas 5.2 and 5.4, we have

$$\begin{aligned} \|E_{\Gamma_i}^{(k)}u\|_{H^1(\Omega_k)}^2 &\lesssim H_k^2 \|\widehat{E}_{\Gamma_i}^{(k)}\widehat{u}\|_{L^2(\widehat{\Omega})}^2 + |\widehat{E}_{\Gamma_i}^{(k)}\widehat{u}|_{H^1(\widehat{\Omega})}^2 \lesssim (p^{-1}H_k^2\eta + p\eta^{-1}) \|\widehat{u}\|_{L^2(\widehat{\Gamma}_i^{(k)})}^2 + p^{-1}\eta |\widehat{u}|_{H^1(\widehat{\Gamma}_i^{(k)})}^2 \\ &\lesssim (p^{-1}H_k\eta + pH_k^{-1}\eta^{-1}) \|u\|_{L^2(\Gamma_i)}^2 + p^{-1}H_k\eta |u|_{H^1(\Gamma_i)}^2 \lesssim (h_{k(\Gamma_i)} + h_{k(\Gamma_i)}^{-1}) \|u\|_{L^2(\Gamma_i)}^2 + h_{k(\Gamma_i)} |u|_{H^1(\Gamma_i)}^2, \end{aligned}$$

which implies the desired result since $h_{k(\Gamma_i)} \leq H_{k(\Gamma_i)} \leq \text{diam } \Omega \lesssim 1$. \square

Since $u \in H_0^1(\Gamma_i)$ vanishes on the two adjacent vertices and since η is chosen such that $\psi_\eta(1) = 0$, we immediately have

Lemma 5.11. *Let Ω_k be a patch and let Γ_i be one of its edges, i.e., $i \in \mathbb{E}(\Omega_k)$. Then, $E_{\Gamma_i}^{(k)}u$ vanishes on all other edges and on all vertices of Ω_k , i.e.,*

$$(E_{\Gamma_i}^{(k)}u)|_{\Gamma_j} = 0 \quad \text{and} \quad (E_{\Gamma_i}^{(k)}u)(\mathbf{x}_m) = 0 \quad \text{for all } u \in H_0^1(\Gamma_i), j \in \mathbb{E}(\Omega_k) \setminus \{i\} \text{ and } m \in \mathbb{V}(\Omega_k).$$

5.5 Overall error estimate

To obtain the overall error estimate (Theorem 5.1), assume that u to a arbitrary but fixed smooth function $\Omega \rightarrow \mathbb{R}$. In the following, we construct a function $u_h \in V_h$ such that the H^1 -error satisfies the corresponding result. First, define $u_{0,h}$ by patch-wise interpolation:

$$u_{0,h} \in L^2(\Omega) \quad \text{such that} \quad u_{0,h}|_{\Omega_k} := u_{0,h}^{(k)} := \Pi_h^{(k)}(u|_{\Omega_k}).$$

Using (23), we obtain

$$\sum_{k=1}^K \|u - u_{0,h}\|_{H^1(\Omega_k)}^2 \lesssim \sum_{k=1}^K h_k^{2q_k} \|u\|_{H^{1+q_k}(\Omega_k)}^2. \quad (33)$$

Following (16), we know that $u_{0,h}^{(k)}(\mathbf{x}_m) = u(\mathbf{x}_m) = u_{0,h}^{(\ell)}(\mathbf{x}_m)$ if \mathbf{x}_m is a common corner of Ω_k and Ω_ℓ ($m \in \mathbb{C}(\Omega_k) \cap \mathbb{C}(\Omega_\ell)$), i.e., that $u_{0,h}$ is continuous across the corners. However, for $m \in \mathbb{T}(\Omega_k)$, we have $u_{0,h}^{(k)}(\mathbf{x}_m) \neq u(\mathbf{x}_m)$ in general. In order to guarantee continuity at T-junctions as well, we define a corrected version of $u_{0,h}$ as follows:

$$u_{1,h} \in L^2(\Omega) \quad \text{such that} \quad u_{1,h}|_{\Omega_k} := u_{1,h}^{(k)} := u_{0,h}^{(k)} + \sum_{m \in \mathbb{C}(\Omega_k) \cap \mathbb{T}} E_{\mathbf{x}_m}^{(k)}(u_{0,h}^{(k)}(\mathbf{x}_m) - u_{0,h}^{(k)}(\mathbf{x}_m)). \quad (34)$$

The function $u_{1,h}$ is continuous at the vertices and satisfies the same error estimate as in (33).

Lemma 5.12. *For any two patches Ω_k and Ω_ℓ with common vertex \mathbf{x}_m ($m \in \mathbb{V}(\Omega_k) \cap \mathbb{V}(\Omega_\ell)$), we have $u_{1,h}^{(k)}(\mathbf{x}_m) = u_{1,h}^{(\ell)}(\mathbf{x}_m)$.*

Proof. We have $u_{1,h}^{(k)}(\mathbf{x}_m) = u_{0,h}^{(k(\mathbf{x}_m))}(\mathbf{x}_m)$ for all $k \in \mathbb{P}(\mathbf{x}_m)$, due to the following observations.

If $m \in \mathbb{C}$, using Lemma 5.9 and (16) we have that $u_{1,h}^{(k)}(\mathbf{x}_m) = u_{0,h}^{(k)}(\mathbf{x}_m) = u(\mathbf{x}_m)$ for all $k \in \mathbb{P}(\mathbf{x}_m)$, including $k(\mathbf{x}_m)$. Now, consider the case $m \in \mathbb{T}$. If k is such that $m \in \mathbb{C}(\Omega_k)$, we have using Lemma 5.9 and the effects of extension that $u_{1,h}^{(k)}(\mathbf{x}_m) = u_{0,h}^{(k(\mathbf{x}_m))}(\mathbf{x}_m)$. If k is such that $m \in \mathbb{T}(\Omega_k)$, using Lemma 5.9 and $k = k(\mathbf{x}_m)$, we have that $u_{1,h}^{(k)}(\mathbf{x}_m) = u_{0,h}^{(k(\mathbf{x}_m))}(\mathbf{x}_m)$. The last two statements guarantee continuity at \mathbf{x}_m if it is a T-junction. \square

Lemma 5.13. *Let $u_{1,h}$ be defined as in (34). Then, the following estimate holds:*

$$\sum_{k=1}^K \|u - u_{1,h}\|_{H^1(\Omega_k)}^2 \lesssim \sum_{k=1}^K h_k^{2q_k} \|u\|_{H^{1+q_k}(\Omega_k)}^2.$$

Proof. Using (34), the triangle inequality, $|\mathbb{C}(\Omega_k) \cap \mathbb{T}| \leq 4$, Lemma 5.7 and (16), we have

$$\begin{aligned} \|u - u_{1,h}\|_{H^1(\Omega_k)}^2 &\lesssim \|u - u_{0,h}\|_{H^1(\Omega_k)}^2 + \sum_{m \in \mathbb{C}(\Omega_k) \cap \mathbb{T}} \|E_{\mathbf{x}_m}^{(k)}(u_{0,h}^{(k(\mathbf{x}_m))})(\mathbf{x}_m) - u(\mathbf{x}_m)\|_{H^1(\Omega_k)}^2 \\ &\lesssim \|u - u_{0,h}\|_{H^1(\Omega_k)}^2 + \sum_{m \in \mathbb{C}(\Omega_k) \cap \mathbb{T}} |u_{0,h}^{(k(\mathbf{x}_m))}(\mathbf{x}_m) - u(\mathbf{x}_m)|^2. \end{aligned}$$

By rearranging the sums and using Assumption 3.2 we obtain

$$\sum_{k=1}^K \|u - u_{1,h}\|_{H^1(\Omega_k)}^2 \lesssim \sum_{k=1}^K \|u - u_{0,h}\|_{H^1(\Omega_k)}^2 + \sum_{k=1}^K \sum_{m \in \mathbb{T}(\Omega_k)} |u_{0,h}^{(k)}(\mathbf{x}_m) - u(\mathbf{x}_m)|^2.$$

Using (34) for the first term and Lemma 5.5, (23) and (24) for the second term, we obtain the desired result. \square

In order to guarantee continuity across the edges as well, we define

$$u_{2,h} \in L^2(\Omega) \quad \text{such that} \quad u_{2,h}|_{\Omega_k} := u_{2,h}^{(k)} := u_{1,h}^{(k)} + \sum_{i \in \mathbb{E}(\Omega_k)} E_{\Gamma_i}^{(k)}(u_{1,h}^{(k(\Gamma_i))} - u_{1,h}^{(k)}). \quad (35)$$

We obtain the desired continuity statement, as well as the desired error estimate.

Lemma 5.14. *We have $u_{2,h} \in C^0(\Omega)$.*

Proof. Since the edge corrections vanish on all corners (Lemma 5.11), we have $u_{2,h}^{(k)}(\mathbf{x}_m) = u_{1,h}^{(k)}(\mathbf{x}_m)$, so continuity across vertices is retained. Using Lemma 5.11, we immediately obtain $u_{2,h}^{(k)}|_{\Gamma_i} = u_{1,h}^{(k(\Gamma_i))}|_{\Gamma_i}$ for all $i \in \mathbb{E}(\Omega_k)$ and all patches Ω_k , i.e., continuity across edges. This shows continuity of the overall function. \square

Lemma 5.15. *Let $u_{2,h}$ be defined as in (35). Then, the following estimate holds:*

$$\sum_{k=1}^K \|u - u_{2,h}\|_{H^1(\Omega_k)}^2 \lesssim \sum_{k=1}^K h_k^{2q_k} \|u\|_{H^{1+q_k}(\Omega_k)}^2.$$

Proof. Using (35), the triangle inequality, the fact that there are at most 4 extensions active on each patch (there are only 4 indices $i \in \mathbb{E}(\Omega_k)$ such that $k \neq k(\Gamma_i)$) and $h_{k(\Gamma_i)} \leq H_{k(\Gamma_i)} \leq \text{diam } \Omega \lesssim 1$, we have

$$\begin{aligned} \|u - u_{2,h}\|_{H^1(\Omega_k)}^2 &\lesssim \|u - u_{1,h}\|_{H^1(\Omega_k)}^2 + \sum_{i \in \mathbb{E}(\Omega_k)} \|E_{\Gamma_i}^{(k)}(u_{1,h}^{(k(\Gamma_i))}) - u_{1,h}^{(k)}\|_{H^1(\Omega_k)}^2 \\ &\lesssim \|u - u_{1,h}\|_{H^1(\Omega_k)}^2 + \sum_{i \in \mathbb{E}(\Omega_k)} \|u_{1,h}^{(k(\Gamma_i))} - u_{1,h}^{(k)}\|_{\Gamma_i}^2, \end{aligned}$$

where we define $\|w\|_{\Gamma_i}^2 := h_{k(\Gamma_i)}|w|_{H^1(\Gamma_i)}^2 + h_{k(\Gamma_i)}^{-1}\|w\|_{L^2(\Gamma_i)}^2$ for convenience. In order to estimate the jumps $u_{1,h}^{(k(\Gamma_i))} - u_{1,h}^{(k)}$, we use (34). We observe that vertex corrections are only performed for vertices \mathbf{x}_m that are T-junctions. If \mathbf{x}_m is a corner both of Ω_k and $\Omega_{k(\Gamma_i)}$ ($m \in \mathbb{C}(\Omega_k) \cap \mathbb{C}(\Omega_{k(\Gamma_i)})$), then $E_{\mathbf{x}_m}^{(k)}$ and $E_{\mathbf{x}_m}^{(k(\Gamma_i))}$ agree on Γ_i . So, there can only be a contribution if $m \in \mathbb{T}(\Omega_k)$ or $m \in \mathbb{T}(\Omega_{k(\Gamma_i)})$. Since $\Omega_{k(\Gamma_i)}$ has the smaller trace space, only the latter case can occur. Thus, we have

$$\|u_{1,h}^{(k(\Gamma_i))} - u_{1,h}^{(k)}\|_{\Gamma_i}^2 \lesssim \|u_{0,h}^{(k(\Gamma_i))} - u_{0,h}^{(k)}\|_{\Gamma_i}^2 + \sum_{m \in \mathbb{V}(\Gamma_i) \cap \mathbb{T}(\Omega_{k(\Gamma_i)})} \|E_{\mathbf{x}_m}^{(k)}(u_{0,h}^{(k(\Gamma_i))})(\mathbf{x}_m) - u_{0,h}^{(k)}(\mathbf{x}_m)\|_{\Gamma_i}^2.$$

Here, the first summand is estimated using (17) and (18). For estimating the second summand, we use $h_{k(\mathbf{x}_m)} = h_{k(\Gamma_i)}$ and Lemma 5.8. So, we obtain

$$\|u_{1,h}^{(k(\Gamma_i))} - u_{1,h}^{(k)}\|_{\Gamma_i}^2 \lesssim \|u_{0,h}^{(k(\Gamma_i))} - u_{0,h}^{(k)}\|_{\Gamma_i}^2 + \sum_{m \in \mathbb{V}(\Gamma_i) \cap \mathbb{T}(\Omega_{k(\Gamma_i)})} |u_{0,h}^{(k(\Gamma_i))}(\mathbf{x}_m) - u_{0,h}^{(k)}(\mathbf{x}_m)|^2.$$

By rearranging the sums and using $h_k \leq h_{k(\Gamma_i)}$ for all $i \in \mathbb{E}(\Omega_k)$, we have

$$\begin{aligned} \sum_{k=1}^K \|u - u_{2,h}\|_{H^1(\Omega_k)}^2 &\lesssim \sum_{k=1}^K \|u - u_{1,h}\|_{H^1(\Omega_k)}^2 + \sum_{k=1}^K \sum_{i \in \mathbb{E}(\Omega_k)} (h_k^{-1} \|u - u_{0,h}^{(k)}\|_{L^2(\Gamma_i)}^2 + h_k \|u - u_{0,h}^{(k)}\|_{H^1(\Gamma_i)}^2) \\ &\quad + \sum_{k=1}^K \sum_{m \in \mathbb{T}(\Omega_k)} |u_{0,h}^{(k)}(\mathbf{x}_m) - u_{0,h}^{(k)}(\mathbf{x}_m)|^2. \end{aligned}$$

Here, the first summand is estimated with Lemma 5.13 and the other summands are estimated using Lemma 5.3 and Lemma 5.5, respectively. Combined with (22), (23) and (24) we obtain the desired result. \square

Proof of Theorem 5.1. Using Lemma 5.14 and $u_{2,h}^{(k)} \in V_h^{(k)}$ for all k , we have $u_{2,h} \in V_h$. Thus, the desired statement follows for smooth u directly from Lemma 5.15. For $u \in \mathcal{H}^{1+q}(\Omega)$, the result follows using standard density arguments. \square

5.6 Overall error estimate for the low-regularity case

In this section, we show Theorem 5.2. We again assume that u is an arbitrary but fixed smooth function first. Since we do not know that the function to be approximated is in $H^2(\Omega)$, we cannot use the projector $\Pi_h^{(k)}$, since that projector is not stable in $H^{1+q}(\Omega)$ for $q < 1$. Instead, we define $u_{0,h}$ by

patch-wise interpolation using a standard $H^1(\Omega)$ -orthogonal projector. So, let $\widehat{\pi}_h^{(k)} : H^1(\widehat{\Omega}) \rightarrow \widehat{V}_h^{(k)}$ be the projector that is orthogonal with respect to the $H^1(\widehat{\Omega})$ -scalar product. Again, define $\pi_h^{(k)}$ via the pull-back principle, i.e., $\pi_h^{(k)} u = (\widehat{\pi}_h^{(k)}(u \circ G_k)) \circ G_k^{-1}$ and $u_{0,h}$ as follows:

$$u_{0,h} \in L^2(\Omega) \quad \text{such that} \quad u_{0,h}|_{\Omega_k} := u_{0,h}^{(k)} := \pi_h^{(k)}(u|_{\Omega_k}).$$

Using the results from [17] and Lemma 5.2, we know that

$$\|u - u_{0,h}\|_{L^2(\Omega_k)} \lesssim h_k^{1+q_k} |u|_{H^{1+q_k}(\Omega_k)} \quad \text{and} \quad |u - u_{0,h}|_{H^r(\Omega_k)} \lesssim h_k^{q_k-r} |u|_{H^{1+q_k}(\Omega_k)} \quad (36)$$

for all $q_k \in \{0, 1, \dots, p\}$ and $r \in \{1, 2\}$ with $r \leq q_k$. Again, the Hilbert space interpolation theorem [1, Theorem 7.23] provides

$$\|u - u_{0,h}\|_{H^{1+\varepsilon}(\Omega_k)} \lesssim h_k^{q_k-\varepsilon} |u|_{H^{1+q_k}(\Omega_k)} \quad (37)$$

for all $q_k \in (0, p]$ and $\varepsilon \in (0, \min_k q_k)$. From standard Sobolev space embedding theorems [1, Theorem 4.12], we know that for all $\varepsilon > 0$ there is a constant $C_\varepsilon \geq 1$ (depending on ε and q_k only) such that

$$\|\widehat{u}\|_{C(\widehat{\Omega})} := \sup_{x \in \widehat{\Omega}} |\widehat{u}(x)| \leq C_\varepsilon \|\widehat{u}\|_{H^{1+\varepsilon}(\widehat{\Omega})} \quad \text{for all } \widehat{u} \in H^{1+\varepsilon}(\widehat{\Omega}).$$

Consequently, using (37) and Lemma 5.2, we also know

$$\|u - u_{0,h}\|_{C(\Omega_k)} \lesssim C_\varepsilon h_k^{q_k-\varepsilon} |u|_{H^{1+q_k}(\Omega_k)} \quad \text{for all } \varepsilon \in (0, q_k). \quad (38)$$

Since $u_{0,h}$ does not interpolate u , we need corrections not only for the T-junctions, but also for the corner vertices. For each vertex \mathbf{x}_m (corner or T-junction), the extension $E_{\mathbf{x}_m,lr}^{(k)}$ is defined via

$$E_{\mathbf{x}_m,lr}^{(k)} s = (\widehat{E}_{\mathbf{x}_m,lr}^{(k)} s) \circ G_k^{-1}, \quad \text{where} \quad (\widehat{E}_{\mathbf{x}_m,lr}^{(k)} s)(\widehat{x}, \widehat{y}) := \psi_{p\widehat{h}_k}(\widehat{x}) \psi_{p\widehat{h}_k}(\widehat{y}) s.$$

As opposed to the case of high regularity, the extension operators do not necessarily match at the edges. Again, using Assumption 3.4, we obtain that $(E_{\mathbf{x}_m,lr}^{(k)} s)(\mathbf{x}_n) = 0$ for $m \neq n$.

We then set

$$u_{1,h} \in L^2(\Omega) \quad \text{such that} \quad u_{1,h}^{(k)} := u_{0,h}^{(k)} + \sum_{m \in \mathbb{C}(\Omega_k)} E_{\mathbf{x}_m,lr}^{(k)}(u_{0,h}^{(k)}(\mathbf{x}_m) - u_{0,h}^{(k)}(\mathbf{x}_m)), \quad (39)$$

where $\mathbf{k}(\mathbf{x}_m)$ is defined as in Section 5.4 if $m \in \mathbb{T}$. If $m \in \mathbb{C}$, then $\mathbf{k}(\mathbf{x}_m) \in \mathbb{P}(\mathbf{x}_m)$ can be chosen arbitrarily. Using the same arguments as in the last section, we observe that $u_{1,h}$ is continuous across all vertices. We obtain the following error estimate.

Lemma 5.16. *Let $u_{1,h}$ be defined as in (39). Then, the following estimate holds:*

$$\sum_{k=1}^K \left(\|u - u_{1,h}\|_{H^1(\Omega_k)}^2 + \|u - u_{1,h}\|_{C(\Omega_k)}^2 \right) \lesssim \sum_{k=1}^K |\mathbb{V}(\Omega_k)| C_\varepsilon h_k^{2(q_k-\varepsilon)} \|u\|_{H^{1+q_k}(\Omega_k)}^2$$

for any $\varepsilon \in (0, \min_k q_k)$.

Proof. Using (39) and Lemmas 5.2 and 5.6, we obtain analogously to the proof of Lemma 5.7:

$$\begin{aligned} \|u - u_{1,h}\|_{H^1(\Omega_k)}^2 &\lesssim \|u - u_{0,h}\|_{H^1(\Omega_k)}^2 + \sum_{m \in \mathbb{V}(\Omega_k)} \|E_{\mathbf{x}_m, lr}^{(k)}(u_{0,h}^{(k(\mathbf{x}_m))})(\mathbf{x}_m) - u_{0,h}^{(k)}(\mathbf{x}_m)\|_{H^1(\Omega_k)}^2 \\ &\lesssim \|u - u_{0,h}\|_{H^1(\Omega_k)}^2 + \sum_{m \in \mathbb{V}(\Omega_k)} |u_{0,h}^{(k(\mathbf{x}_m))}(\mathbf{x}_m) - u_{0,h}^{(k)}(\mathbf{x}_m)|^2. \end{aligned}$$

Since $\|E_{\mathbf{x}_m, lr}^{(k)}s\|_{C(\Omega_k)} = |s|$, we also have

$$\|u - u_{1,h}\|_{C(\Omega_k)}^2 \lesssim \|u - u_{0,h}\|_{C(\Omega_k)}^2 + \sum_{m \in \mathbb{V}(\Omega_k)} |u_{0,h}^{(k(\mathbf{x}_m))}(\mathbf{x}_m) - u_{0,h}^{(k)}(\mathbf{x}_m)|^2.$$

By rearranging the sums and using the triangle inequality $|u_{0,h}^{(k(\mathbf{x}_m))}(\mathbf{x}_m) - u_{0,h}^{(k)}(\mathbf{x}_m)|^2 \lesssim |u(\mathbf{x}_m) - u_{0,h}^{(k(\mathbf{x}_m))}(\mathbf{x}_m)|^2 + |u(\mathbf{x}_m) - u_{0,h}^{(k)}(\mathbf{x}_m)|^2$, we obtain

$$\begin{aligned} \sum_{k=1}^K \left(\|u - u_{1,h}\|_{H^1(\Omega_k)}^2 + \|u - u_{1,h}\|_{C(\Omega_k)}^2 \right) &\lesssim \sum_{k=1}^K \left(\|u - u_{0,h}\|_{H^1(\Omega_k)}^2 + \|u - u_{0,h}\|_{C(\Omega_k)}^2 \right) \\ &\quad + \sum_{m \in \mathbb{V}(\Omega_k)} |u(\mathbf{x}_m) - u_{0,h}^{(k)}(\mathbf{x}_m)|^2. \end{aligned}$$

(36) and (38) give the desired result. \square

To guarantee continuity across edges, we also need edge corrections. Here, we base them on the discrete harmonic extensions, i.e., $\widehat{E}_{\Gamma_i, lr}^{(k)}$ is a linear operator that maps from the trace space $\widehat{V}_h^{(k)}|_{\widehat{\Gamma}_i^{(k)}}$ to $\widehat{V}_h^{(k)}$ that satisfies $|\widehat{E}_{\Gamma_i, lr}^{(k)}\widehat{u}|_{\widehat{\Gamma}_i^{(k)}} = \widehat{u}$ and $|\widehat{E}_{\Gamma_i, lr}^{(k)}\widehat{u}|_{\partial\widehat{\Omega} \setminus \widehat{\Gamma}_i^{(k)}} = 0$ such that it minimizes its $H^1(\widehat{\Omega})$ -seminorm, i.e., $|\widehat{E}_{\Gamma_i, lr}^{(k)}\widehat{u}|_{H^1(\widehat{\Omega})}$. Due to [19, Theorem 4.2, Lemma 4.15], the following estimate holds:

$$|\widehat{E}_{\Gamma_i, lr}^{(k)}\widehat{u}|_{H^1(\widehat{\Omega})} \lesssim p|\widehat{u}|_{H^{1/2}(\partial\widehat{\Omega})} \lesssim p|\widehat{u}|_{H^{1/2}(\widehat{\Gamma}_i^{(k)})} + p(1 + \log \widehat{h}_k^{-1} + \log p)\|\widehat{u}\|_{C(\widehat{\Gamma}_i^{(k)})} \text{ for all } \widehat{u} \in \widehat{V}_h^{(k)}|_{\widehat{\Gamma}_i^{(k)}}.$$

The Poincaré inequality and Lemma 5.2 yield for $E_{\Gamma_i, lr}^{(k)}s = (\widehat{E}_{\Gamma_i, lr}^{(k)}s) \circ G_k^{-1}$ that

$$\|E_{\Gamma_i, lr}^{(k)}u\|_{H^1(\Omega_k)} \lesssim p\|u\|_{H^{1/2}(\Gamma_i)} + p(1 + \log \frac{H_k}{h_k} + \log p)\|u\|_{C(\Gamma_i)} \text{ for all } u \in V_h^{(k)}|_{\Gamma_i}. \quad (40)$$

By construction, we have $(E_{\Gamma_i, lr}^{(k)}u)|_{\Gamma_j} = 0$ and $(E_{\Gamma_i, lr}^{(k)}u)(\mathbf{x}_m) = 0$ for all $u \in V_h^{(k)}|_{\Gamma_i} \cap H_0^1(\Gamma_i)$, all $j \in \mathbb{E}(\Omega_k) \setminus \{i\}$ and $m \in \mathbb{V}(\Omega_k)$. We define

$$u_{2,h} \in L^2(\Omega) \quad \text{such that} \quad u_{2,h}^{(k)} := u_{1,h}^{(k)} + \sum_{i \in \mathbb{E}(\Omega_k)} E_{\Gamma_i, lr}^{(k)}(u_{1,h}^{(k(\Gamma_i))} - u_{1,h}^{(k)}). \quad (41)$$

Analogously to the preceding section, we obtain that $u_{2,h}$ is continuous across all edges and that the continuity across the vertices is retained. The following lemma provides an error estimate.

Lemma 5.17. *Let $u_{2,h}$ be defined as in (41). Then, the following estimate holds:*

$$\sum_{k=1}^K \|u - u_{2,h}\|_{H^1(\Omega_k)}^2 \lesssim C_\varepsilon p \max_\ell (1 + \log \frac{H_\ell}{h_\ell} + \log p) |\mathbb{V}(\Omega_\ell)| \sum_{k=1}^K h_k^{2(q_k - \varepsilon)} \|u\|_{H^{1+q_k}(\Omega_k)}^2.$$

Proof. Using (41) and (40), we obtain

$$\|u - u_{2,h}\|_{H^1(\Omega_k)}^2 \lesssim \|u - u_{1,h}\|_{H^1(\Omega_k)}^2 + p \sum_{i \in \mathbb{E}(\Omega_k)} \|u_{1,h}^{(k(\Gamma_i))} - u_{1,h}^{(k)}\|_{\Gamma_i}^2,$$

where $\|w\|_{\Gamma_i}^2 := \|w\|_{H^{1/2}(\Gamma_i)}^2 + \Lambda \|w\|_{C(\Gamma_i)}^2$ and $\Lambda := \max_\ell (1 + \log \frac{H_\ell}{h_\ell} + \log p)$. Using the triangle inequality ($\|u_{1,h}^{(k(\Gamma_i))} - u_{1,h}^{(k)}\|_{\Gamma_i} \leq \|u - u_{1,h}^{(k(\Gamma_i))}\|_{\Gamma_i} + \|u - u_{1,h}^{(k)}\|_{\Gamma_i}$), by rearranging the local contributions and using $\sum_i \|w\|_{H^{1/2}(\Gamma_i)} \leq \|w\|_{H^{1/2}(\partial\Omega_k)}$, we obtain

$$\sum_{k=1}^K \|u - u_{2,h}\|_{H^1(\Omega_k)}^2 \lesssim \sum_{k=1}^K \|u - u_{1,h}\|_{H^1(\Omega_k)}^2 + \sum_{k=1}^K p (\|u - u_{1,h}^{(k)}\|_{H^{1/2}(\partial\Omega_k)}^2 + \Lambda \|u - u_{1,h}^{(k)}\|_{C(\Omega_k)}^2).$$

Using a standard trace theorem [1, Lemma 7.40], we have

$$\sum_{k=1}^K \|u - u_{2,h}\|_{H^1(\Omega_k)}^2 \lesssim p \Lambda \sum_{k=1}^K (\|u - u_{1,h}\|_{H^1(\Omega_k)}^2 + \|u - u_{1,h}^{(k)}\|_{C(\Omega_k)}^2).$$

Lemma 5.16 gives the desired result. \square

Proof of Theorem 5.2. Since $u_{2,h} \in C^0(\Omega)$ and $u_{2,h}^{(k)} \in V_h^{(k)}$ for all k , we have $u_{2,h} \in V_h$. Thus, the desired statement follows directly from Lemma 5.17 for u smooth. For $u \in \mathcal{H}^{1+q}(\Omega)$, the result follows using standard density arguments. \square

6 Numerical experiments

6.1 L-shape domain

As a first test case, we apply our approach for adaptive IgA to an L-shaped domain $\Omega = (-1, 1)^2 \setminus ([0, 1] \times [-1, 0])$. Since the domain is non-convex, we cannot expect full H^2 -regularity of the solution, even if $f \in L^2(\Omega)$ and $g \in H^{3/2}(\partial\Omega)$.

The singularity in the solution is however local and known to be at the reentrant corner. By using adaptive refinement, we are able to reconstruct the expected order of convergence one would expect for the used spline space.

First, we prescribe a solution $u(x, y) = u(r \cos \varphi, r \sin \varphi) = r^{2/3} \sin(\frac{2}{3}\varphi)$, where r and ϕ are radial coordinates and consider the following Poisson problem:

$$-\Delta \phi = 0 \quad \text{in } \Omega, \tag{42}$$

$$\phi = u|_{\partial\Omega} \quad \text{on } \partial\Omega. \tag{43}$$

It is straightforward to show that u solves (42)-(43), however it holds only that $u \in H^{4/3}(\Omega)$.

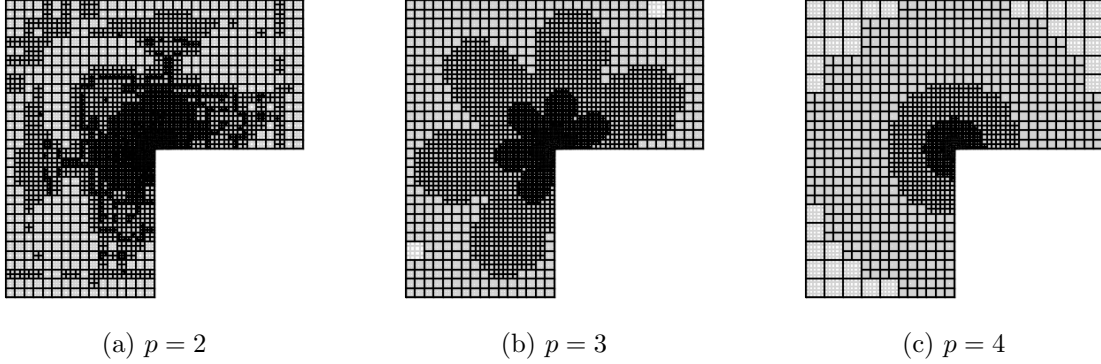


Figure 6: Final mesh for the first L-domain test case.

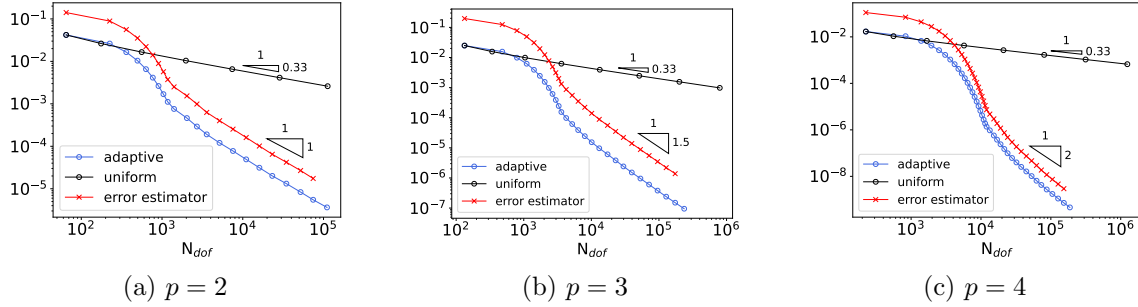


Figure 7: H^1 -error for the first L-domain test case.

We represent the L-domain with 3 conforming patches, where each patch is discretized by spline spaces of maximum smoothness and $p + 1$ uniformly distributed knots in each coordinate, where p is the spline degree. We further employ the residual error estimator (3) on every patch. The final meshes that were obtained with adaptive refinement are depicted in Figure 6. In Figure 7, the H^1 -error and the value of the error estimator are presented. For the case of uniform refinement (black curve), one can see that the error decays like $h^{2/3} \approx N_{dof}^{-1/3}$, which is consistent with the global regularity result $u \in H^{1+1/3}(\Omega)$. In case of adaptive refinement, one obtains for $p = 2, 3, 4$ that – after some faster pre-asymptotic behavior – the H^1 -error (blue curve) behaves like $N_{dof}^{-2/p}$, which is the best one would expect for these spline degrees. The curve representing the error indicator (red curve) is parallel to that representing the H^1 -error. Analogously, in Figure 8, one can see that the L^2 -error in case of uniform refinement decays like $h^{4/3} \approx N_{dof}^{-2/3}$. Using adaptivity, one can recover the full rate $N_{dof}^{-2/(p+1)}$.

Additionally we solved the Poisson problem on the L-domain with constant source and homogeneous boundary conditions, i.e. we solve

$$\begin{aligned} -\Delta\phi &= 1 && \text{in } \Omega, \\ \phi &= 0 && \text{on } \partial\Omega. \end{aligned}$$

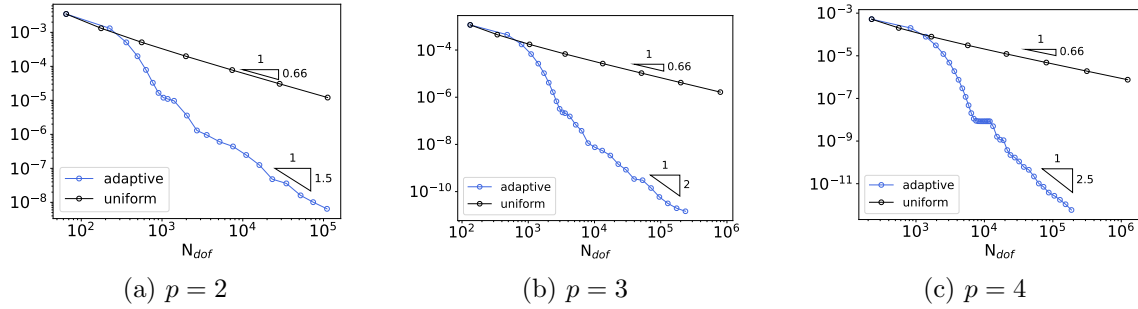


Figure 8: L^2 -error for the first L-domain test case.

In this case, we do not know an exact solution in closed form. Since the right-hand side is smooth, the solution will be smooth in the interior as well. This does not extend to the boundary of the domain Ω , particularly its corners. In the following we present the final mesh configuration for different polynomial degrees p .

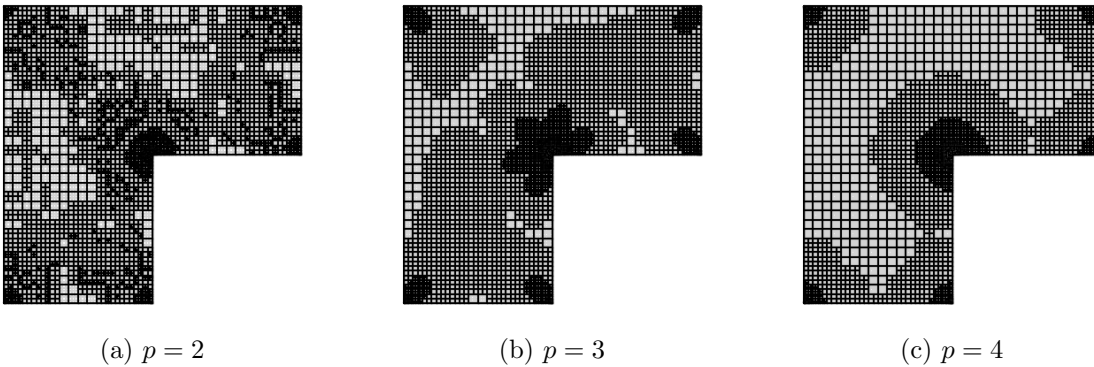


Figure 9: Final mesh for the second L-domain test case.

For this example, Figures 10 and 11 indicate that we obtain the same convergence behavior as for the first test case. In Figure 9, one can spot the difference to the first example. In the first example, the adaptive refinement algorithm has only refined towards the reentrant corner, since by construction the manufactured solution has a singularity only there. In the second example, one can see that also patches close to the regular corners of Ω are refined.

6.2 Electric Motor

We also apply the adaptive scheme to a (rather simplistic) electric motor, where the electromagnetic phenomena are prescribed by Maxwell's equations. In this example, we consider linear magneto-statics. For given permeability μ , current density J and permanent magnetization M , the magnetic field density H and the magnetic flux density B are given by

$$\text{curl } H = J, \quad \text{div } B = 0, \quad B = \mu(H + M).$$

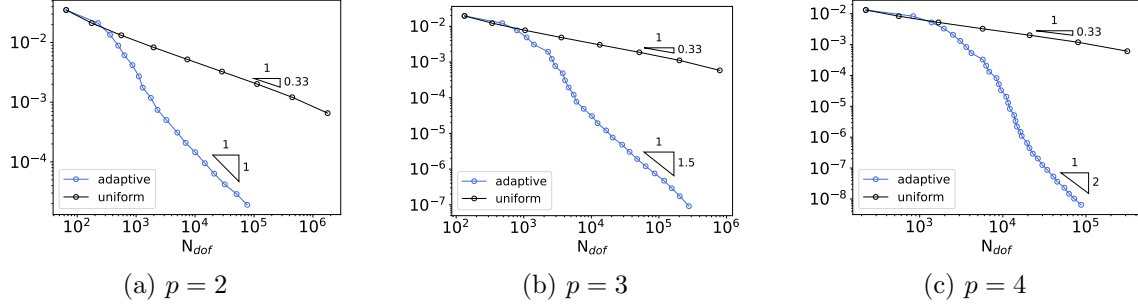


Figure 10: H^1 -error for the second L-domain test case.

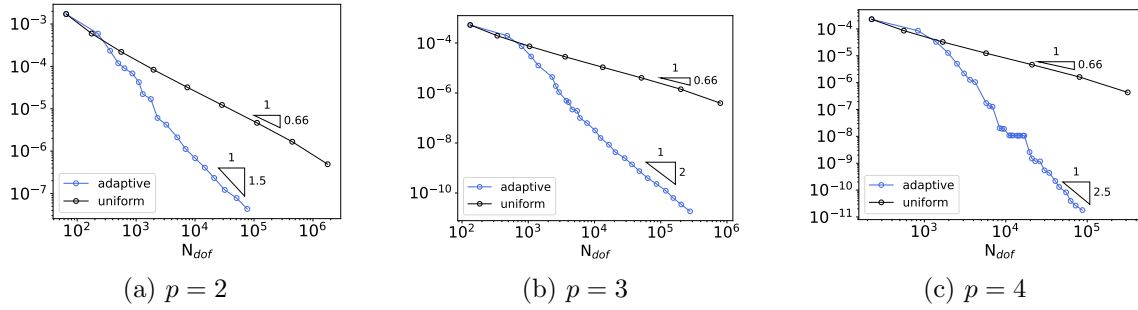


Figure 11: L^2 -error for the second L-domain test case.

If the computational domain $\Omega \subset \mathbb{R}^3$ is simply connected, the condition $\operatorname{div} B = 0$ implies the existence of a vector potential A such that $B = \operatorname{curl} A$. Assuming that $\Omega = \Omega_0 \times [0, L]$, $H = (H_1, H_2, 0)^\top$, $B = (B_1, B_2, 0)^\top$, $A = (0, 0, u)^\top$, $J = (0, 0, j)^\top$ and $M = (M_1, M_2, 0)^\top$ the problem further simplifies to a scalar problem on the cross-section Ω_0 , depicted in Figure 12 (a). Here, we solve for the potential $u \in H_D^1(\Omega) := \{v \in H^1(\Omega) : v|_{\Gamma_D} = 0\}$ that satisfies

$$\begin{aligned} -\operatorname{div}(\mu^{-1} \nabla u) &= j + \operatorname{div} M^\perp && \text{in } \Omega_0, \\ u &= 0 && \text{on } \Gamma_D, \\ \mu^{-1} \nabla u + M^\perp &= 0 && \text{on } \Gamma_N, \end{aligned}$$

in a weak sense, where $M^\perp := (M_2, -M_1)^\top$. The Neumann condition on Γ_N , colored in red in Figure 12 (a), represents a periodicity assumption. The Dirichlet condition on $\Gamma_D = \partial\Omega_0 \setminus \Gamma_N$, colored in blue, represents an isolation in the magnetic flux. We choose the current density $j = 0$ on the whole domain, i.e., the electric motor is unpowered. The permeability μ is defined piecewise depending on the material. For the air (white), we have $\mu_{\text{Air}} = 4\pi \cdot 10^{-7}$, for the iron (gray) $\mu_{\text{Iron}} = 204\pi \cdot 10^{-5}$, for the permanent magnet (yellow) $\mu_{\text{Mag}} = 4.344\pi \cdot 10^{-7}$. So, we have jumps in the coefficient μ^{-1} of approximately the magnitude 10^4 . The permanent magnetization on the magnet area (M vanishes everywhere else) is given by $M = \rho \mu_{\text{Mag}}^{-1} \mathbf{n}$, where $\rho = 1.28$ is the magnetic remanence and \mathbf{n} is the unit vector perpendicular to the centerline of the magnet. The direction of \mathbf{n} is alternated between consecutive magnets.

The initial patch configuration used for discretization of the variational problem is depicted in

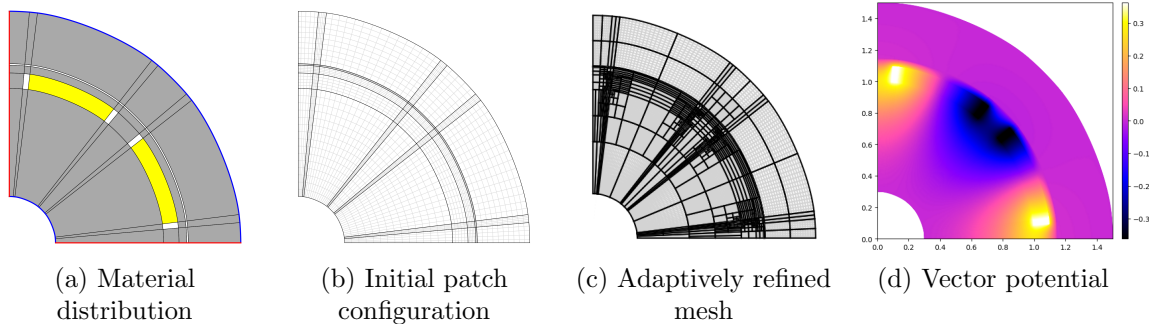


Figure 12: Electrical motor.

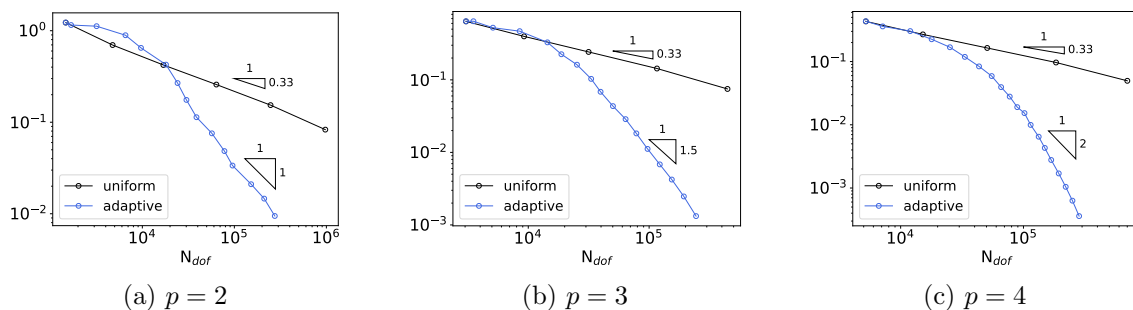


Figure 13: Error in energy norm for the electrical motor.

Figure 12 (b), where the patch boundaries are the black lines and the inner knot mesh is shown in light gray. One can see that the domain does not have reentrant corners that would reduce the smoothness of the solution. However, the material parameters vary significantly, which again reduces the smoothness of the solution. The solution is depicted in Figure 12 (d); it was computed on the adaptive mesh seen in Figure 12 (c). The Figures 13 and 14 show that the convergence rates are again reduced if we use uniform refinement. Since the singularities are caused by 90-degree corners adjacent to the permanent magnets, the error in the energy norm converges like $h^{2/3} \approx N_{dof}^{-1/3}$ and the L^2 error like $h^{4/3} \approx N_{dof}^{-2/3}$. The full rate that would be expected for the spline degree $p = 2$ is again obtained by using the adaptive approach. For higher spline degrees ($p = 3, 4$) we even seem to observe superconvergent rates, however, this might still be in the pre-asymptotic regime.

7 Conclusions

We proposed a new approach to employ adaptive mesh refinement in the framework of multi-patch Isogeometric Analysis that allows to re-use computational frameworks for the handling of multi-patch geometries that are already well-established. Specifically, on each patch, the tensor-product structure of the B-spline basis is retained. Since our approach increases the number of patches, we introduce additional interfaces that are only C^0 continuous. This, however, only marginally increases the number of degrees of freedom compared to alternative methods (like HB- or THB-

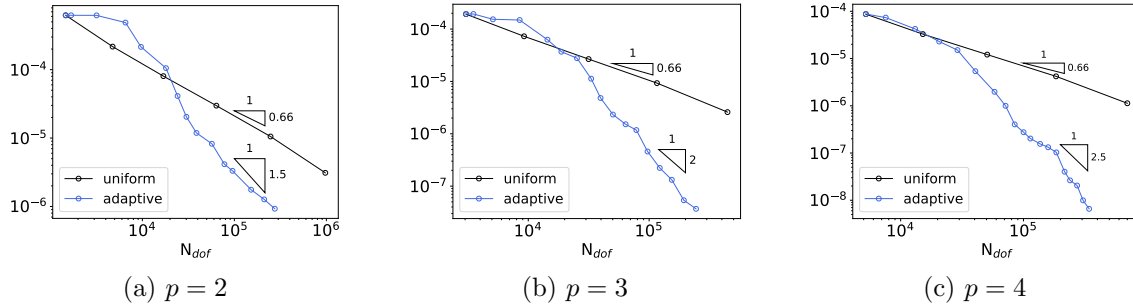


Figure 14: L^2 -error for the electrical motor.

splines or T-splines). Since it reduces the overlap between the supports of basis functions of different mesh levels, our approach is both simpler and can be implemented in a more efficient way. Through the subdivision of local patches into sub-patches, hanging nodes are emerging, which leads to non-matching discretizations along common interfaces. These discretizations are coupled through constraints on each edge, yielding a H^1 -conforming function space.

For practical computations, a basis of the overall space might be desired. We have developed an algorithm that uses these constraints and constructs a basis for the whole spline space. Since it is purely matrix based, it can be extended to 3D effortlessly. The constructed global basis retains all important properties of the local spline bases, like the non-negativity of the basis functions, that they form a partition of unity and have local support.

Additionally we gave an a-priori approximation error analysis by constructing a suitable quasi-interpolation operator. For the high regularity case ($u \in H^2(\Omega)$), we could even show p -robustness. An analogous result is obtained for the low regularity case ($u \in H^{1+q}(\Omega)$ with $q \in (0, 1)$), however its dependence on the parameters seems not to be sharp. We further gave some numerical examples confirming applicability of adaptive schemes with our approach of patch-subdivision.

References

- [1] Robert A. Adams and John J. F. Fournier. *Sobolev spaces*. eng. 2nd edition. Pure and applied mathematics. Elsevier Academic Press, 2003.
- [2] Peter Binev, Wolfgang Dahmen, and Ron DeVore. “Adaptive finite element methods with convergence rates”. In: *Numerische Mathematik* 97 (2 2004), pp. 219–268.
- [3] Carl de Boor. “On calculating with B-splines”. In: *Journal of Approximation Theory* 6 (1 July 1972), pp. 50–62.
- [4] Francesco Calabrò, Giancarlo Sangalli, and Mattia Tani. “Fast formation of isogeometric Galerkin matrices by weighted quadrature”. In: *Computer Methods in Applied Mechanics and Engineering* 316 (2017), pp. 606–622.
- [5] J. Austin Cottrell, Thomas J.R. Hughes, and Yuri Bazilevs. *Isogeometric Analysis: Toward Integration of CAD and FEA*. Wiley, 2009.
- [6] Willy Dörfler. “A convergent adaptive algorithm for Poisson’s equation”. In: *SIAM Journal on Numerical Analysis* 33 (3 1996), pp. 1106–1124.

- [7] Carlotta Giannelli, Bert Jüttler, and Hendrik Speleers. “THB-splines: The truncated basis for hierarchical splines”. In: *Computer Aided Geometric Design* 29 (7 Oct. 2012), pp. 485–498.
- [8] Carlotta Giannelli et al. “THB-splines: An effective mathematical technology for adaptive refinement in geometric design and isogeometric analysis”. In: *Computer Methods in Applied Mechanics and Engineering* 299 (2016), pp. 337–365.
- [9] Clemens Hofreither and Stefan Takacs. “Robust multigrid for isogeometric analysis based on stable splittings of spline spaces”. In: *SIAM Journal on Numerical Analysis* 55 (4 2017), pp. 2004–2024.
- [10] Thomas J. R. Hughes, J. Austin Cottrell, and Yuri Bazilevs. “Isogeometric analysis: CAD, finite elements, NURBS, exact geometry and mesh refinement”. In: *Computer Methods in Applied Mechanics and Engineering* 194 (39 2005), pp. 4135–4195.
- [11] Kjetil André Johannessen, Trond Kvamsdal, and Tor Dokken. “Isogeometric analysis using LR B-splines”. In: *Computer Methods in Applied Mechanics and Engineering* 269 (2014), pp. 471–514.
- [12] Rainer Kraft. “Adaptive and Linearly Independent Multilevel B-Splines”. In: *Surface Fitting and Multiresolution Methods*. Ed. by A. Le Méhauté, C. Rabut, and L. L. Schumaker. 1997, pp. 209–218.
- [13] Ulrich Langer and Ioannis Touloupoulos. “Analysis of multipatch discontinuous Galerkin IgA approximations to elliptic boundary value problems”. In: *Computing and Visualization in Science* 17 (5 2015), pp. 217–233.
- [14] Ulrich Langer et al. “Multipatch discontinuous galerkin isogeometric analysis”. In: vol. 107. 2015, pp. 219–268.
- [15] Angelos Mantzafaris et al. “Low rank tensor methods in Galerkin-based isogeometric analysis”. In: *Computer Methods in Applied Mechanics and Engineering* 316 (2017), pp. 1062–1085.
- [16] Carl-Martin Pfeiler and Dirk Praetorius. “Dörfler marking with minimal cardinality is a linear complexity problem”. In: *Mathematics of Computation* 89 (326 2020), pp. 2735–2752.
- [17] Espen Sande, Carla Manni, and Hendrik Speleers. “Ritz-type projectors with boundary interpolation properties and explicit spline error estimates”. In: *Numerische Mathematik* 151 (2 2022), pp. 475–494.
- [18] Giancarlo Sangalli and Mattia Tani. “Isogeometric preconditioners based on fast solvers for the sylvester equation”. In: *SIAM Journal on Scientific Computing* 38 (6 2016), A3644–A3671.
- [19] Rainer Schneckleitner and Stefan Takacs. “Condition number bounds for IETI-DP methods that are explicit in p and h ”. In: *Mathematical Models and Methods in Applied Sciences* 30.11 (2020), pp. 2067–2103.
- [20] Thomas W. Sederberg et al. “T-spline simplification and local refinement”. In: 2004, pp. 276–283.
- [21] Stefan Takacs. “Robust approximation error estimates and multigrid solvers for isogeometric multi-patch discretizations”. In: *Mathematical Models and Methods in Applied Sciences* 28 (10 2018), pp. 1899–1928.

- [22] Stefan Takacs and Thomas Takacs. “Approximation error estimates and inverse inequalities for B-splines of maximum smoothness”. In: *Mathematical Models and Methods in Applied Sciences* 26 (7 2016), pp. 1411–1445.
- [23] Rüdiger Verfürth. *A posteriori error estimation techniques for finite element methods*. Oxford University Press, 2013.